

1 **Investigating the Links Between Ozone and Organic**  
2 **Aerosol Chemistry in a Biomass Burning Plume from a**  
3 **Prescribed Fire in California Chaparral**

4 **M. J. Alvarado<sup>1</sup>, C. R. Lonsdale<sup>1</sup>, R. J. Yokelson<sup>2</sup>, S. K. Akagi<sup>2</sup>, H. Coe<sup>3</sup>, J. S.**  
5 **Craven<sup>4</sup>, E. V. Fischer<sup>5</sup>, G. R. McMeeking<sup>5</sup>, J. H. Seinfeld<sup>4</sup>, T. Soni<sup>1,\*</sup>, J. W.**  
6 **Taylor<sup>3</sup>, D. R. Weise<sup>6</sup>, and C. E. Wold<sup>7</sup>**

7 [1]{Atmospheric and Environmental Research, Lexington, MA, USA}

8 [2]{Department of Chemistry, University of Montana, Missoula, MT, USA}

9 [3]{Centre for Atmospheric Science, University of Manchester, Manchester, UK}

10 [4]{Division of Chemistry and Chemical Engineering, California Institute of Technology,  
11 Pasadena, CA, USA}

12 [5]{Department of Atmospheric Science, Colorado State University, Fort Collins, CO, USA}

13 [6]{PSW Research Station, USDA Forest Service, Riverside, CA, USA}

14 [7]{Fire Sciences Laboratory, United States Department of Agriculture (USDA) Forest  
15 Service, Missoula, MT, USA}

16 [\*]{now at: Shell Chemical LP, Houston, Texas, USA}

17

18 Correspondence to: M. J. Alvarado (malvarad@aer.com)

19

20 **Abstract**

21 Within minutes after emission, complex photochemistry in biomass burning smoke plumes  
22 can cause large changes in the concentrations of ozone (O<sub>3</sub>) and organic aerosol (OA). Being  
23 able to understand and simulate this rapid chemical evolution under a wide variety of  
24 conditions is a critical part of forecasting the impact of these fires on air quality, atmospheric  
25 composition, and climate. Here we use version 2.1 of the Aerosol Simulation Program (ASP)  
26 to simulate the evolution of O<sub>3</sub> and secondary organic aerosol (SOA) within a young biomass  
27 burning smoke plume from the Williams prescribed burn in chaparral, which was sampled  
28 over California in November 2009. We demonstrate the use of a method for simultaneously

1 accounting for the impact of the unidentified intermediate volatility, semi-volatile, and  
2 extremely low volatility organic compounds (here collectively called “SVOCs”) on the  
3 formation of OA (using the Volatility Basis Set) and O<sub>3</sub> (using the concept of mechanistic  
4 reactivity). We show that this method can successfully simulate the observations of O<sub>3</sub>, OA,  
5 NO<sub>x</sub>, C<sub>2</sub>H<sub>4</sub>, and OH to within measurement uncertainty using reasonable assumptions about  
6 the average chemistry of the unidentified SVOCs. These assumptions were: (1) a reaction rate  
7 constant with OH of  $\sim 10^{-11}$  cm<sup>3</sup>/s; (2) a significant fraction (up to  $\sim 50\%$ ) of the RO<sub>2</sub> + NO  
8 reaction resulted in fragmentation, rather than functionalization, of the parent SVOC; (3)  $\sim 1.1$   
9 molecules of O<sub>3</sub> were formed for every molecule of SVOC that reacted; (4)  $\sim 60\%$  of the OH  
10 that reacted with the unidentified NMOC was regenerated as HO<sub>2</sub>, and (5) that  $\sim 50\%$  of the  
11 NO that reacted with the SVOC peroxy radicals was lost, presumably to organic nitrate  
12 formation. Additional evidence for the fragmentation pathway is provided by the observed  
13 rate of formation of acetic acid, which is consistent with our assumed fragmentation rate.  
14 However, the model overestimates PAN formation downwind by about 50%, suggesting the  
15 need for further refinements to the chemistry. This method could provide a way for  
16 classifying different smoke plume observations in terms of the average chemistry of their  
17 SVOCs, and could be used to study how the chemistry of these compounds (and the O<sub>3</sub> and  
18 OA they form) varies between plumes.

## 19 **1 Introduction**

20 Biomass burning is a major source of atmospheric trace gases and particles that impact air  
21 quality and climate (e.g., Crutzen and Andreae, 1990; van der Werf, 2010; Akagi et al., 2011).  
22 Within minutes after emission, rapid and complex photochemistry within the young biomass  
23 burning smoke plumes can lead to significant increases in the concentrations of secondary  
24 pollutants such as ozone (O<sub>3</sub>, e.g. Mauzerall et al., 1998; Goode et al., 2000; Hobbs et al.,  
25 2003; Pfister et al., 2006; Lapina et al., 2006; Val Martin et al., 2006; Yokelson et al., 2009;  
26 Jaffe and Widger, 2012; Akagi et al., 2012; 2013), peroxyacetyl nitrate (PAN, e.g. Jacob et  
27 al., 1992; Alvarado et al., 2010, 2011; Fischer et al., 2014), and organic aerosol (OA, e.g.  
28 Hobbs et al., 2003; Grieshop et al., 2009a,b; Yokelson et al., 2009; Hennigan et al., 2011;  
29 Heringa et al., 2011; Vakkari et al., 2014), while other smoke plumes can show little to no  
30 formation of O<sub>3</sub> (e.g. Alvarado et al., 2010, Zhang et al., 2014) or OA (e.g. Akagi et al.,  
31 2012). Understanding the atmospheric chemistry of these young smoke plumes, especially  
32 which conditions can lead to the secondary formation of O<sub>3</sub>, PAN, and OA, is thus critical to

1 understanding the impact of these plumes on atmospheric composition and the resulting  
2 impacts on air quality, human health, and climate. However, global- and regional-scale  
3 Eulerian models of atmospheric chemistry artificially dilute biomass burning emissions into  
4 large-scale grid boxes, which can result in large errors in the predicted concentrations of O<sub>3</sub>  
5 and aerosol species downwind (e.g., Alvarado et al., 2009; Zhang et al., 2014). In contrast,  
6 plume-scale Lagrangian models allow us to examine the chemical and physical  
7 transformations within these concentrated plumes in detail and can be used to develop  
8 parameterizations for this aging process for coarser models (e.g., the parameterizations of  
9 Vinken et al., 2011 and Holmes et al., 2014 for ship plumes).

10 Our understanding of the formation of ozone within biomass burning plumes is still poor, due  
11 both to the limited observational data available on O<sub>3</sub> formation in smoke plumes and the  
12 highly variable results seen in the available observations. Several aircraft and surface studies  
13 of the chemistry of young biomass burning smoke plumes have found significant formation of  
14 O<sub>3</sub> within smoke plumes. For example, Baylon et al. (2014) reported  $\Delta O_3/\Delta CO$  from 0.4% to  
15 11%, corresponding to O<sub>3</sub> enhancements of 3.8 to 32 ppbv in 19 wildfire plumes samples at  
16 Mt. Bachelor Observatory. They note that plumes that have low values of  $\Delta O_3/\Delta CO$  can still  
17 correspond to significant O<sub>3</sub> enhancements in concentrated plumes, with one event with a  
18  $\Delta O_3/\Delta CO$  value of 0.81% corresponding to an O<sub>3</sub> enhancement of 17 ppbv. Akagi et al.  
19 (2013) found significant O<sub>3</sub> formation ( $\Delta O_3/\Delta CO$  from 10-90%) within two hours for all of  
20 the South Carolina prescribed fires studied, and Parrington et al. (2013) found values of  
21  $\Delta O_3/\Delta CO$  increased from  $2.0 \pm 0.8\%$  in boreal biomass burning plumes less than 2 days old  
22 over Eastern Canada to  $55 \pm 29\%$  in plumes that were more than 5 days old. Similarly, Andreae  
23 et al. (1994) found that aged plumes (over 10 days old) from the biomass burning regions of  
24 South America and Africa had  $\Delta O_3/\Delta CO$  values between 20-70%. However, other studies,  
25 mainly in boreal regions, have found little formation or even depletion of O<sub>3</sub> in some young  
26 biomass burning plumes (e.g., Alvarado et al., 2010). This low O<sub>3</sub> formation is likely due to a  
27 combination of low emissions of NO<sub>x</sub> from the boreal fires (Akagi et al., 2011), sequestration  
28 of NO<sub>x</sub> in PAN and other organic nitrates (e.g., Jacob et al., 1992; Alvarado et al., 2010,  
29 2011), and reduced rates of photochemical reactions due to aerosol absorption and scattering  
30 (e.g. Jiang et al., 2012). Similarly, some studies have shown that fires can contribute to high  
31 surface O<sub>3</sub> events that exceed the US air quality standard for O<sub>3</sub> (e.g., Jaffe et al., 2013), while  
32 other studies suggest that this enhanced surface O<sub>3</sub> is only present when the biomass burning  
33 emissions mix with anthropogenic pollution (Singh et al., 2012; Zhang et al., 2014). However,

1 even given the observed variability among fires, it is likely that biomass burning has an  
2 impact on the concentrations of tropospheric O<sub>3</sub>. For example, the recent review of Jaffe and  
3 Widger (2012) estimated that biomass burning could contribute 170 Tg of O<sub>3</sub> per year,  
4 accounting for 3.5% of all global tropospheric O<sub>3</sub> production. However, Sudo and Akimoto  
5 (2007) estimated that over a third of tropospheric O<sub>3</sub> came from free troposphere chemical  
6 production due to biomass burning outflow from South America and South Africa.

7 The NO<sub>x</sub> emitted by biomass burning is rapidly converted into a wide variety of inorganic  
8 nitrate (i.e. HNO<sub>3(g)</sub> and total aerosol inorganic nitrate, or NO<sub>3(p)</sub>) and organic nitrate species  
9 (i.e. alkyl nitrates (RONO<sub>2</sub>) and peroxy nitrates (RO<sub>2</sub>NO<sub>2</sub>), including PAN; Jacob et al., 1992;  
10 Yokelson et al., 2009; Alvarado et al., 2010, 2011; Akagi et al., 2012). The rate at which this  
11 conversion occurs and the relative production of inorganic nitrate, alkyl nitrates, and peroxy  
12 nitrates are a key control of the impact of the biomass burning on O<sub>3</sub> production and  
13 atmospheric composition. Once NO<sub>x</sub> is converted to inorganic or organic nitrate, it is  
14 generally unavailable for further O<sub>3</sub> formation near the fire source. Furthermore, while  
15 conversion of NO<sub>x</sub> into inorganic nitrate (HNO<sub>3(g)</sub> + NO<sub>3(p)</sub>) is generally irreversible (except  
16 for the slow reaction of HNO<sub>3(g)</sub> with OH), peroxy nitrate species like PAN can act as  
17 thermally unstable reservoirs of NO<sub>x</sub>, allowing transport of NO<sub>x</sub> in the upper atmosphere far  
18 from the original source and then producing NO<sub>x</sub> via thermal decomposition as the airmass  
19 descends to the surface (e.g., Fischer et al., 2010). This regenerated NO<sub>x</sub> can thus impact O<sub>3</sub>  
20 formation far from the original source.

21 In addition, photochemistry within the smoke plume can rapidly oxidize non-methane organic  
22 compounds (NMOCs), both those that were emitted in the gas phase and those emitted in the  
23 particle phase, lowering their vapor pressure and thus leading to the formation of secondary  
24 organic aerosol (SOA). As with O<sub>3</sub> and PAN formation, the formation of SOA in smoke  
25 plumes is highly variable, with the ratio of OA to CO<sub>2</sub> increasing by a factor of 2-3 downwind  
26 of some biomass burning fires (e.g. Hobbs et al., 2003; Grieshop et al., 2009a,b; Yokelson et  
27 al., 2009; Hennigan et al., 2011; Heringa et al., 2011; Vakkari et al., 2014), while in others it  
28 can stay constant or even decrease (e.g. Capes et al., 2008; Akagi et al., 2012). For cases  
29 where little net SOA formation was observed, it is likely that the NMOCs were still being  
30 oxidized. However, in these cases the fragmentation of the organic species after oxidation  
31 (leading to higher volatility products) is likely more common than functionalization (i.e. the  
32 addition of oxygen to the organic species, leading to lower volatility products).

1 Plume-scale Lagrangian parcel models can be used to investigate the evolution of O<sub>3</sub>, PAN,  
2 and OA in smoke plumes in detail, as their relatively simple parameterizations of plume  
3 dispersion and transport allow detailed simulation of the chemical and microphysical  
4 processes taking place within the young smoke plumes (e.g., Mauzerall et al., 1998; Mason et  
5 al., 2001, 2006; Jost et al., 2003; Trentmann et al., 2005; Alvarado and Prinn, 2009; Arnold et  
6 al., 2014; Heilman et al., 2014). Previous plume-scale modeling studies have greatly advanced  
7 our understanding of these transformations. Mauzerall et al. (1998) found that O<sub>3</sub> production  
8 within biomass burning plumes was limited by the concentration of NO<sub>x</sub> and that the  
9 formation and subsequent degradation of peroxy acetyl nitrate (PAN) helped to maintain NO<sub>x</sub>  
10 concentrations. Mason et al. (2001) and Trentmann et al. (2003) showed that oxygenated  
11 volatile organic compounds (OVOCs) were critical to the formation of O<sub>3</sub> within the smoke  
12 plumes. More recent work has suggested heterogeneous chemistry and currently unidentified  
13 organic species as potential explanations for the rapid formation of O<sub>3</sub> and organic aerosol  
14 seen within some smoke plumes (Trentmann et al., 2005; Mason et al., 2006; Alvarado and  
15 Prinn, 2009).

16 The Aerosol Simulation Program (ASP) was developed to simulate the formation of ozone  
17 and secondary organic aerosol (SOA) within young biomass burning plumes (Alvarado,  
18 2008). ASP v1.0 was used to simulate several African and North American plumes (Alvarado  
19 and Prinn, 2009) and to simultaneously simulate the chemistry, dynamics, and radiative  
20 transfer within a smoke plume using a high-resolution three-dimensional plume model  
21 (Alvarado et al., 2009). Alvarado and Prinn (2009) showed while their initial ASP v1.0  
22 simulations underestimated the formation of both OH and O<sub>3</sub> in the Timbavati savannah fire  
23 smoke plume (Hobbs et al., 2003), if the OH concentration in ASP v1.0 was fixed at the  
24 estimated value of  $1.7 \times 10^7$  molecules/cm<sup>3</sup> then the model was able to reproduce the  
25 observed concentrations of O<sub>3</sub>. This suggested that the model was missing an important  
26 source of OH, and they proposed a heterogeneous reaction of NO<sub>2</sub> on aerosol particles  
27 producing HONO, followed by the photolysis of HONO into NO and OH, as a candidate for  
28 the missing source of OH within the smoke plume. Alvarado and Prinn (2009) also found that  
29 including only SOA formation from known SOA precursors (mainly aromatic species like  
30 toluene) underestimated the concentrations of organic aerosol observed downwind by ~60%,  
31 suggesting that the model was missing a large source of SOA. They proposed that the large  
32 amount of gas-phase organic compounds that were unidentified by the then current  
33 measurement techniques (Christian et al., 2003; Warneke et al., 2011) could include the

1 precursors for the missing SOA. Assuming these compounds had SOA yields similar to  
2 monoterpenes gave the observed SOA formation.

3 In this paper, we describe recent updates to the gas-phase chemistry and secondary organic  
4 aerosol (SOA) formation modules in ASP. We use this updated version (ASP v2.1) to  
5 simulate the chemical evolution of a young biomass burning smoke plume sampled over  
6 California in November near San Luis Obispo (the Williams fire, Akagi et al., 2012). The  
7 analysis of the O<sub>3</sub>, PAN, and OA evolution in biomass burning plumes is complicated by the  
8 fact that a large fraction (30-50% by carbon mass, Christian et al., 2003; Warneke et al., 2011)  
9 of the NMOCs present in smoke plumes are unidentified, and thus their oxidation chemistry is  
10 not well known.

11 Furthermore, while there was clear secondary formation of O<sub>3</sub> and PAN within the Williams  
12 fire plume, the dilution-corrected amount of OA in the plume decreased slightly (Akagi et al.,  
13 2012). Most current methods for modeling the OA evolution in smoke plumes lead to  
14 significant secondary growth of the OA (e.g., Grieshop et al., 2009a), but we need instead to  
15 modify ASP v2.1 to simulate both this slight loss of OA and the chemical formation of O<sub>3</sub>,  
16 PAN, and other gas-phase species.

17 Here we present a method for simultaneously accounting for the impact of the unidentified  
18 organic compounds (here collectively called “SVOCs”) on the formation of OA and O<sub>3</sub>,  
19 drawing on the Volatility Basis Set approach (e.g., Robinson et al., 2007) for modeling OA  
20 and the concept of the mechanistic reactivity of a mixture of organic compounds (e.g., Carter,  
21 1994). We show that this method can successfully simulate the Williams fire plume  
22 observations using reasonable assumptions about the chemistry of the unidentified SVOCs.

23 Section 2 describes the updates to the gas-phase chemistry and secondary organic aerosol  
24 formation modules of ASP for version 2.1. Section 3 discusses our validation of the gas-phase  
25 chemistry in ASP v2.1 against data from a smog chamber (Carter et al., 2005). Section 4  
26 describes the Williams fire and summarizes the available observations of the smoke plume  
27 from Akagi et al. (2012). Section 5 discusses the results of the ASP simulation of the  
28 Williams fire, including sensitivity tests to investigate the chemistry of the unidentified  
29 SVOCs and their impacts on O<sub>3</sub>, PAN, other trace gases, and OA, while Section 6 gives the  
30 conclusions of our study and directions for future work.

## 1   **2   Updates to the Aerosol Simulation Program (ASP)**

2   An overview of ASP v1.0 is given by Alvarado and Prinn (2009), and the routines are  
3   described in detail in Alvarado et al. (2008). Here we briefly discuss the modules of ASP that  
4   have not changed since Alvarado and Prinn (2009) in Section 2.1 before describing the  
5   updates to the gas-phase chemistry (Section 2.2) and SOA formation (Section 2.3) routines for  
6   ASP v2.1.

### 7   **2.1   ASP Modules**

8   Aerosols are represented in ASP by a single moving-center sectional size distribution, where  
9   the aerosol concentrations are distributed over increments in radius space (Jacobson 1997,  
10   2002, 2005). ASP includes modules to calculate aerosol thermodynamics, gas-to-aerosol mass  
11   transfer (condensation/evaporation), and coagulation of aerosols. The thermodynamics  
12   module in ASP uses the Mass Flux Iteration (MFI) method of Jacobson (2005) to calculate the  
13   equilibrium concentration of gas and aerosol species. Equilibrium constants for the inorganic  
14   electrolyte reactions match those of Fountoukis and Nenes (2007). Binary activity coefficients  
15   of inorganic electrolytes are calculated using the Kusik-Meissner method (Kusik and  
16   Meissner, 1978; Resch, 1995), as are the mean activity coefficients. The water content of  
17   inorganic aerosols is calculated with an iterative routine that calculates water activities for  
18   aqueous solutions of a single electrolyte using a formula based on the Gibbs-Duhem equation  
19   (Steele, 2004). Steele (2004) and Alvarado (2008) found this approach compares well with  
20   other inorganic aerosol thermodynamics models such as ISORROPIA (Nenes et al., 1998;  
21   Fountoukis and Nenes, 2007).

22   Mass transfer between the gas and aerosol phases is calculated in ASP using a hybrid scheme  
23   where the flux-limited kinetic equations governing the condensation/evaporation of H<sub>2</sub>SO<sub>4</sub>  
24   and organic species are integrated, whereas NH<sub>3</sub>, HNO<sub>3</sub>, and HCl are assumed to be in  
25   equilibrium (Alvarado, 2008). Aerosol coagulation is calculated using the semi-implicit  
26   scheme of Jacobson (2005) with a Brownian coagulation kernel.

### 27   **2.2   Gas-phase Chemistry Updates**

28   The gas-phase chemistry within the ASP model for Version 2.1 has been completely revised  
29   from ASP v1.0, which used the CalTech Atmospheric Chemistry Mechanism (CACM, Griffin  
30   et al., 2005). The revised ASP v2.1 gas phase chemical mechanism includes 1608 reactions

1 between 621 species. Examples of the gas-phase species input file and the reaction  
2 mechanism input file for ASP v2.1, along with other key chemical input files, are included in  
3 the Supplemental Material.

4 All inorganic gas-phase chemistry within ASP v2.1 was updated to follow the IUPAC  
5 recommendations (Atkinson et al., 2004; updated data downloaded from [http://iupac.pole-  
7 ether.fr/](http://iupac.pole-<br/>6 ether.fr/), accessed June 2012). We also tested the JPL recommendations (Evaluation #17,  
8 Sander et al., 2011) for these rate constants, but found that the differences between the  
9 recommendations generally made little difference to the model simulations, and as the IUPAC  
10 values were closer to those in ASP v1.0, these values were used.

11 All gas-phase chemistry for organic compounds containing 4 carbons or less has been  
12 “unlumped,” i.e. the chemistry for each individual organic compound is explicitly resolved.  
13 This was done by following the reactions of the Leeds Master Chemical Mechanism (MCM)  
14 v3.2 (<http://mcm.leeds.ac.uk/MCM/>, accessed June 2012; Jenkin et al., 1997, 2003; Saunders  
15 et al., 2003; Bloss et al., 2005) for these species.

16 The chemical mechanism of isoprene within ASP v2.1 has been updated to follow the Paulot  
17 et al. (2009a,b) isoprene scheme, as implemented in GEOS-Chem and including corrections  
18 based on more recent studies (e.g., Crouse et al., 2011, 2012). The (lumped) chemistry for all  
19 other organic compounds in ASP has been updated to follow the Regional Atmospheric  
20 Chemistry Mechanism (RACM) v2 (Goliff et al., 2013). We chose RACM2 over the SAPRC-  
21 07 (Carter, 2010) and CB05 (Yarwood et al., 2005) lumped chemical mechanisms as the  
22 treatment of peroxy radicals in the RACM2 mechanism was more similar to the treatment in  
23 the Leeds MCM and the Paulot isoprene scheme, resulting in a more consistent chemical  
24 mechanism for ASP v2.1.

25 Photolysis rates are calculated offline using the Tropospheric Ultraviolet and Visible (TUV)  
26 radiation model version 5.0 (Madronich and Flocke, 1998) for 15 minute increments, which  
27 are then linearly interpolated in ASP. Alvarado and Prinn (2009) assumed a “clear sky”  
28 radiation field that ignored the effect of aerosol absorption and scattering on the calculated  
29 photolysis rates. Here we instead estimate the time-dependent aerosol, O<sub>3</sub>, SO<sub>2</sub>, and NO<sub>2</sub>  
30 concentrations within the smoke plumes and calculate their effect on the photolysis rates at  
31 different heights within the plume. In the TUV simulations, we assume no clouds and that the  
32 initial smoke plume AOD at 330 nm decreases due to dilution assuming a background  
concentration of ~0, and the aerosol is assumed to have a constant (both with time and



1 wavelength) single scattering albedo (SSA) of 0.9 based on the review of AERONET biomass  
2 burning smoke optical property retrievals by Reid et al. (2005a). We also dilute the initial  
3 plume concentrations of the trace gases  $\text{NO}_2$  and  $\text{SO}_2$  assuming a background concentration of  
4  $\sim 0$ , as these species can also absorb ultraviolet and visible (UV-VIS) light and thus can  
5 impact photolysis rates. For the photolysis rate calculations only,  $\text{O}_3$  is assumed to be 0  
6 initially and increased after 15 minutes to a constant value based on the observed formation of  
7  $\text{O}_3$  within the smoke plume. Section 5.1 has more details on the specific approach and  
8 quantitative values used for the Williams Fire.

### 9 **2.3 SOA Formation Updates**

10 We have updated the SOA formation module to follow the semi-empirical Volatility Basis Set  
11 (VBS) model of Robinson et al. (2007). Our implementation of this scheme followed the  
12 approach used by Ahmadov et al. (2012) to link the VBS scheme with the RACM chemical  
13 mechanism within WRF-Chem. We use 9 surrogates or “bins” for semi-volatile, intermediate  
14 volatility, low volatility, and extremely low volatility organic compounds (hereafter  
15 collectively referred to as “SVOCs” for simplicity) as in Dzepina et al., 2009, rather than only  
16 4 as in Ahmadov et al. (2012). The saturation mass concentration at 300 K ( $C^*$ , see Robinson  
17 et al., 2007) of each SVOC bin differs by a factor of 10, and covers the range from 0.01 to  
18  $1.0 \times 10^6 \mu\text{g}/\text{m}^3$ . Note that “SVOC” as defined in this paper includes both semivolatile organic  
19 compounds ( $C^*$  between  $10^{-2}$  and  $10^3 \mu\text{g m}^{-3}$ ) and intermediate volatility organic compounds  
20 (species with  $C^*$  between  $10^4$  and  $10^6 \mu\text{g m}^{-3}$ ) as defined in Dzepina et al. (2009), but we refer  
21 to both of these species classes collectively as “SVOCs” rather than as “S/IVOCs” as in  
22 Dzepina et al. (2009) for simplicity. Following the Model to Predict the Multiphase  
23 Partitioning of Organics (MPMPO) of Griffin et al. (2003, 2005) and Pun et al. (2002), we  
24 assumed that an aqueous phase and a mixed hydrophobic organic phase are always present in  
25 the aerosol. Partitioning of organics between the gas and hydrophobic phase is governed by  
26 Raoult’s law (assuming that all hydrophobic-phase OM is quasi-liquid and can dissolve  
27 organics as in Pankow, 1994a,b), while partitioning of organics into the aqueous phase is  
28 governed by Henry’s law. Following Pun et al. (2002), we assumed that (1) there is no  
29 interaction between the aqueous phase inorganic ions and the aqueous phase organics, and  
30 thus no organic salt formation, and (2) the activity coefficients of the organic ions (formed by  
31 the dissociation of organic acids) are equivalent to those of the corresponding molecular  
32 solute. We further assumed that the pH of the aqueous phase is dominated by the strong

1 inorganic acids and bases, and that the pH effects of the dissociating organic acids are  
2 negligible.

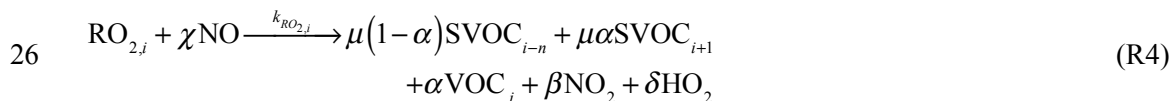
3 Like most organic compounds, SVOCs will react with OH. Most mechanisms for this  
4 chemistry (e.g., Robinson et al., 2007; Dzepina et al., 2009; Grieshop et al., 2009a,b;  
5 Ahmadov et al., 2012) parameterize this chemistry by assuming that the SVOCs react with  
6 OH to form a lower volatility SVOC, as in the reaction:



8 where  $\mu$  is the relative mass gain due to oxidation (e.g. via O addition),  $k_{\text{OH}}$  is the reaction rate  
9 with OH, and  $n$  is the “volatility shift”, or by how many factors of 10 to lower the  $C^*$  of the  
10 product with each OH reaction. This simplified chemistry can be extended to account for the  
11 fact that the SVOCs could fragment during oxidation, leading to higher volatility products:



13 where  $\alpha$  is the fraction of  $\text{SVOC}_i$  that fragments into  $\text{SVOC}_{i+1}$  and  $\text{VOC}_j$ . Shrivastava et al.  
14 (2013) used a similar approach to show that adding SVOC fragmentation to WRF-Chem  
15 simulations of the Mexico City Plateau improved the model’s ability to simulate the observed  
16 concentrations of SOA. However, the highly simplified chemistry of Reactions R1 or R2 is  
17 not appropriate for situations where reactions with the SVOC compounds are a potentially  
18 significant sink of OH, such as in a concentrated smoke plume. Thus in ASP v2.1, the  
19 average, lumped chemistry of the SVOCs is instead parameterized in a more realistic manner  
20 for a generic organic species, following the idea of “mechanistic reactivity” (e.g., Carter,  
21 1994; Bowman and Seinfeld, 1994a,b; Seinfeld and Pandis, 1998). After reaction with OH  
22 SVOCs produce peroxy radicals ( $\text{RO}_2$ ), which can react with NO to form  $\text{NO}_2$  and  $\text{HO}_2$ ,  
23 thereby regenerating OH and forming  $\text{O}_3$ . Reactions R3 and R4 show this more general  
24 chemical mechanism for the SVOCs:



1 where  $k_{RO_2,i}$  is assumed to be  $4.0 \times 10^{-12} \text{ cm}^3 \text{ molecule}^{-1} \text{ s}^{-1}$  based on the reaction rate for the  
 2 peroxy radicals from long-chain alkanes and alkenes with NO in RACM2 (Goliff et al., 2013).  
 3 We can see that  $\chi - \beta$  is the number of  $\text{NO}_x$  lost (implicitly via the addition of a nitrate group to  
 4 the product SVOCs),  $1 - \delta$  is the number of  $\text{HO}_x$  lost, and  $\beta + \delta$  is the number of  $\text{O}_3$  made per  
 5 reaction (by subsequent reactions of  $\text{NO}_2$  and  $\text{HO}_2$  to generate  $\text{O}_3$ ). For example, the values  
 6 for long-chain alkanes (HC8) in the RACM<sub>2</sub> mechanism (Goliff et al., 2013) would be  $\chi = 1$ ,  $\delta$   
 7  $= 0.63$ , and  $\beta = 0.74$ , such that 0.26  $\text{NO}_x$  and 0.37  $\text{HO}_x$  are lost and 1.37  $\text{O}_3$  are formed per  
 8 reaction. Note that the mechanism of Reactions R3 and R4 is still highly simplified: we  
 9 assume that reaction of SVOC with OH always produces a  $\text{RO}_2$  radical, and that the  $\text{RO}_2$   
 10 produced does not react with  $\text{HO}_2$  or another  $\text{RO}_2$ . Also note that Reactions R3 and R4  
 11 represent the average chemistry of the unknown species collectively, and may not apply to  
 12 any individual species in that mixture. Our purpose is less to detail all the possible reactions  
 13 of the unidentified SVOCs and more to explore how their average chemistry might affect  $\text{O}_3$   
 14 and OA evolution in smoke plumes. The specific combinations of parameters for Reactions  
 15 R3 and R4 that were evaluated in this study are shown in Table 2.

16 We also adjusted the calculation of aerosol water content to use the “kappa” ( $\kappa$ )  
 17 parameterization of organic hygroscopicity (Petters and Kreidenweis, 2007) for the lumped  
 18 SVOCs. In this parameterization, the hygroscopicity parameter  $\kappa$  for the organic species is  
 19 defined as:

$$20 \quad \frac{1}{a_w} = 1 + \kappa \frac{V_{s,i}}{V_{w,i}} \quad (1)$$

21 where  $a_w$  is the activity of water in the solution (equal to the relative humidity at equilibrium),  
 22  $V_{s,i}$  is the volume of the dry organic solute  $i$  and  $V_{w,i}$  is the volume of water in the solution.  
 23 The water content calculated for each organic species, along with that calculated for the  
 24 inorganic solution ( $V_{w,inorg}$  see Section 2.1 above) are then combined using the Zdanovskii,  
 25 Stokes, and Robinson (ZSR) approximation (Zdanovskii, 1948; Stokes and Robinson, 1966):

$$26 \quad V_w = \frac{a_w}{1 - a_w} \sum_i \kappa_i V_{s,i} + V_{w,inorg} \quad (2)$$

### 1 3 ASP Photochemistry Evaluated with Smog Chamber Data

2 To evaluate the performance of the updated photochemical mechanism in ASP v2.1 in  
3 predicting the formation of ozone, several test simulations were performed to compare the  
4 results of the mechanism to laboratory smog chamber data. This comparison provides us with  
5 a baseline for interpreting the results of our simulation of O<sub>3</sub> formation in the Williams Fire in  
6 Section 5. The data used for the comparison came from the EPA chamber of Carter et al.  
7 (2005), which consists of two collapsible 90 m<sup>3</sup> FEP Teflon reactors (chambers A and B).

8 Table S1 in the Supplemental Material shows the temperature and initial reactant  
9 concentrations used in our model to simulate each chamber study. All model simulations were  
10 performed at a pressure of 1000 mbar, a relative humidity of 1%, and a CH<sub>4</sub> concentration of  
11 1800 ppbv. The temperature and concentration data were provided by William P.L. Carter  
12 (<http://www.cert.ucr.edu/~carter/SAPRC/SAPRCfiles.htm>, accessed March 2014). The EPA  
13 chamber runs used an 8 compound surrogate for ambient VOC concentrations, consisting of  
14 formaldehyde, ethylene, propene, trans-2-butene, n-butane, n-octane, toluene, and m-xylene  
15 (Carter et al., 1995, 2005). The initial concentrations of HONO were extrapolated from CO-  
16 NO<sub>x</sub> and n-butane-NO<sub>x</sub> runs to account for the potential chamber radical source (Carter et al.,  
17 2005).

18 Table S2 in the Supplemental Material presents the rates of off-gassing (i.e., re-emission of  
19 HCHO and other species from the walls of the reaction chamber), wall reaction rates, and  
20 selected photolysis rates for the chamber experiments considered here. The off-gassing rate  
21 for HONO was determined as the rate that enabled the SAPRC-99 chemical mechanism  
22 (Carter, 2000) to best predict the O<sub>3</sub> formation observed in CO-air, HCHO-air and CO-  
23 HCHO-air experiments performed within the chamber (Carter et al., 2005). The rate in  
24 Chamber A was found to be slightly higher than that in Chamber B, so different values are  
25 used for the chambers. The off-gassing rate of HCHO was chosen to match the low but  
26 measurable amount of formaldehyde found even in pure air and CO-NO<sub>x</sub> experiments in the  
27 chamber. Heterogeneous wall loss reaction rates for O<sub>3</sub>, NO<sub>2</sub>, and N<sub>2</sub>O<sub>5</sub> were also estimated  
28 from reactor observations (Carter et al., 2005). The photolysis rate of NO<sub>2</sub> in the chambers  
29 was measured directly, and scaling factors for the other photolysis rates were calculated by  
30 Carter et al. (2005) from the relative spectral intensity of the arc lamp.

31 Following Carter et al. (2005), we evaluated the ability of our mechanism to simulate the total  
32 amount of NO oxidized and O<sub>3</sub> formed in the experiments, measured as  $\Delta([\text{O}_3] - [\text{NO}])_t \equiv$

1  $([O_3]_t - [NO]_t) - ([O_3]_{\text{initial}} - [NO]_{\text{initial}})$ . The hourly results of the comparisons for  $\Delta([O_3] -$   
2  $[NO])$  are presented in Figure 1. We can see that the ASP v2.1 mechanism tends to  
3 underestimate  $\Delta([O_3] - [NO])$ , with a mean absolute bias of -24.6 ppbv and a mean  
4 normalized bias of -22.4%. Comparisons of the ASP calculations for  $O_3$ ,  $NO$ , and  $NO_x$  (not  
5 shown) show that this model underestimate of  $\Delta([O_3] - [NO])$  is primarily due to the model  
6 underestimating  $O_3$  formation, rather than underestimating the loss of  $NO$  or  $NO_x$ . Similarly,  
7 the ASP v2.1 calculations for the concentrations of the organic gas species matches well with  
8 the chamber measurements (not shown) except for formaldehyde (HCHO), where the  
9 secondary formation of HCHO appears to be underestimated. Figure 2 shows the bias in  
10  $\Delta([O_3] - [NO])$  versus the initial ratio of the mixing ratio of reactive organic gases (ROGs,  
11 e.g., the concentration of the surrogate gases in ppm C) to the mixing ratio of  $NO_x$  (in ppm  
12 N). We can see that the bias is between 0% and -10% for  $ROG/NO_x$  ratios greater than 30, but  
13 increases to -40% to -50% for “high  $NO_x$ ” cases ( $ROG/NO_x$  ratios  $\ll 20$ ). For comparison,  
14 the initial  $ROG/NO_x$  ratio in biomass burning smoke can range from  $\sim 10$ -100 ppm C/ppm N  
15 (Akagi et al., 2011, assuming that the total NMOC mass is 1.6 times the mass of carbon in  
16 these compounds). Both the general underestimation of  $\Delta([O_3] - [NO])$  and the increase of  
17 the negative bias at low  $ROG/NO_x$  concentrations is consistent with the behaviors of the  
18 SAPRC-99 (Carter et al., 2005), SAPRC-07 (Carter, 2010), and CB05 (Yarwood et al., 2005)  
19 mechanisms evaluated against the EPA chamber data. Carter (2010) noted that this under-  
20 prediction of  $O_3$  at low  $ROG/NO_x$  ratios was apparently linked to the presence of aromatics in  
21 the surrogate mixture, with comparisons of SAPRC-07 with EPA chamber runs with a non-  
22 surrogate mixture showing a positive bias of about +25% for cases with low  $ROG/NO_x$  ratios.

#### 23 **4 Williams Fire Data**

24 The Williams Fire (34°41'45'' N, 120°12'23'' W) was sampled by the US Forest Service  
25 (USFS) Twin Otter aircraft from 10:50-15:20 LT on November 17, 2009 (Akagi et al., 2012).  
26 The fire burned approximately 81 hectares of scrub oak woodland understory and coastal sage  
27 scrub. Skies were clear all day and RH was low (11-26%) with variable winds (2-5 m s<sup>-1</sup>). The  
28 Williams Fire smoke plume showed significant secondary production of  $O_3$  and PAN, but the  
29 enhancement ratio of OA to  $CO_2$  decreased slightly downwind (Akagi et al., 2012). In this  
30 study, we use the processed data from Akagi et al. (2012) that provided concentrations of  
31 several trace gases and OA measured during several quasi-Lagrangian transects of the  
32 Williams fire. Full details on the measurements made and the processing of the data for the

1 plume transects are given in Akagi et al. (2012); those used in this study are briefly described  
2 here.

### 3 **4.1 Airborne Fourier Transform InfraRed spectrometer (AFTIR)**

4 The University of Montana AFTIR system and the instruments described below were  
5 deployed on a US Forest Service (USFS) Twin Otter aircraft. The AFTIR (Yokelson et al.,  
6 1999, 2003) was used to measure 21 gas-phase species, including carbon dioxide (CO<sub>2</sub>),  
7 carbon monoxide (CO), nitric oxide (NO), nitrogen dioxide (NO<sub>2</sub>), nitrous acid (HONO),  
8 peroxy acetyl nitrate (PAN), ozone (O<sub>3</sub>), glycolaldehyde (HCOCH<sub>2</sub>OH), ethylene (C<sub>2</sub>H<sub>4</sub>),  
9 formaldehyde (HCHO), acetic acid (CH<sub>3</sub>COOH), and formic acid (HCOOH). IR spectra were  
10 collected at 1 Hz. “Grab samples” of air were selected by closing the valves for 1–2 min to  
11 allow signal averaging, and the resulting IR spectra were analyzed to quantify all detectable  
12 compounds.

### 13 **4.2 Aerosol Mass Spectrometer (AMS)**

14 An Aerodyne compact time-of-flight (CToF) aerosol mass spectrometer (herein referred to as  
15 AMS) measured aerosol chemical composition in a repeating cycle for 4 out of every 12 s  
16 during flight, including within the smoke plume. The AMS has been described in great detail  
17 elsewhere (Drewnick et al., 2005; Canagaratna et al., 2007). An isokinetic particle inlet  
18 sampling fine particles with a diameter cut-off of a few microns (Yokelson et al., 2007;  
19 Wilson et al., 2004) supplied the AMS. As the AMS does not measure super-micron particles,  
20 the inlet transmission should not have affected the results. A collection efficiency of 0.5  
21 (Huffman et al., 2005; Drewnick et al., 2003; Allan et al., 2004) was applied to the AMS data,  
22 which were processed to retrieve the mass concentration for the major non-refractory particle  
23 species: OA, non-sea salt chloride, nitrate, sulfate, and ammonium, with <36% uncertainty.

### 24 **4.3 Other Measurements**

25 The ambient three-dimensional wind velocity, temperature, relative humidity, and barometric  
26 pressure were measured at a frequency of 1-Hz with a wing-mounted AIMMS-20 probe  
27 (Aventech Research, Inc., Beswick et al., 2008). A non-dispersive infrared instrument NDIR  
28 (LiCor model 7000) measured CO<sub>2</sub> (at 0.5 Hz) from the third channel on the isokinetic  
29 particle inlet that also supplied the AMS.

## 1 5 ASP Simulation of Williams Fire

### 2 5.1 ASP Setup

3 As in Alvarado and Prinn (2009), we simulated the Williams fire smoke plume using ASP  
 4 within a simple Lagrangian parcel model following Mason et al. (2001). We assume a  
 5 Lagrangian parcel of fixed vertical extent ( $H$ , here assumed to be 1 km) and down-trajectory  
 6 length ( $L$ ), but variable cross-trajectory width  $y(t)$ . The temperature and pressure of the parcel  
 7 are assumed to be constant. The full continuity equations for the Lagrangian parcel model are  
 8 then

$$9 \quad \frac{dC_q}{dt} = -\frac{4K_y}{(y_o^2 + 8K_y t)} (C_q - C_q^a) - \frac{v_d}{H} C_q + \left( \frac{dC_q}{dt} \right)_{cond} + \left( \frac{dC_q}{dt} \right)_{chem} \quad (3)$$

$$10 \quad \frac{dn_i}{dt} = -\frac{4K_y}{(y_o^2 + 8K_y t)} (n_i - n_i^a) - \frac{v_d}{H} n_i + \left( \frac{dn_i}{dt} \right)_{cond} + \left( \frac{dn_i}{dt} \right)_{coag} \quad (4)$$

$$11 \quad \frac{dc_{q,i}}{dt} = -\frac{4K_y}{(y_o^2 + 8K_y t)} (c_{q,i} - c_{q,i}^a) - \frac{v_d}{H} c_{q,i} + \left( \frac{dc_{q,i}}{dt} \right)_{cond} + \left( \frac{dc_{q,i}}{dt} \right)_{coag} + \left( \frac{dc_{q,i}}{dt} \right)_{chem} \quad (5)$$

12 where  $C_q$  is the concentration of gas-phase species (molecules  $\text{cm}^{-3}$  air),  $n_i$  is the number  
 13 concentration of particles in size bin  $i$  (particles  $\text{cm}^{-3}$  air),  $c_{q,i}$  is the concentration of aerosol  
 14 species  $q$  in size bin  $i$  (mol  $\text{cm}^{-3}$  air),  $y_o$  is the initial plume width (m), and  $K_y$  represents the  
 15 horizontal diffusivity of the atmosphere ( $\text{m}^2 \text{s}^{-1}$ ). The superscript  $a$  indicates the concentration  
 16 of the given species in the atmosphere outside of the parcel (i.e., the background  
 17 concentration).

18 The first term on the right-hand side of Equations 3-5 represents the effect of plume  
 19 dispersion on the concentrations. Note that  $y_o$  and  $K_y$  can be reduced to a single parameter, the  
 20 initial dilution time scale  $\tau_{mix,o}$ :

$$21 \quad -\frac{4K_y}{(y_o^2 + 8K_y t)} = -\frac{1}{\frac{y_o^2}{4K_y} + 2t} = -\frac{1}{\tau_{mix,o} + 2t} \quad (6)$$

1 The second term on the right hand side of Equations 3-5 is the effect of deposition on the  
2 concentrations, where  $v_d$  is the deposition velocity ( $\text{m s}^{-1}$ ). We set the dry deposition velocity  
3 equal to 0 for gas-phase species, as the plume did not touch the ground during the modeled  
4 period, and use the size-dependent terminal velocity of the aerosol particles as the deposition  
5 velocity for aerosol species assuming a 1 km thick plume. As submicron aerosol dominated  
6 the aerosol mass in the smoke plume, this deposition of aerosol species has a negligible effect  
7 on the results, and given the low relative humidity during the Williams Fire, we also did not  
8 include wet deposition of particles or gases. The remaining terms represent the change in gas-  
9 and particle-phase concentrations due to net mass transfer between the gas and aerosol phases  
10 (*cond*), coagulation of particles (*coag*), and chemical production and loss (*chem*).

11 The observed changes in CO mixing ratio were used to determine the best-fit model initial  
12 dilution time scale ( $\tau_{mix,o} = 106.9$  s) as well as upper and lower limits of the time scale  
13 ( $\tau_{mix,o}(0) = 15.0$  s and 212.2 s, respectively), as shown in Figure 3. Note that this dilution  
14 fitting procedure neglects the impact of the chemical production and loss of CO on the  
15 observed concentrations, but modeling results with an inert tracer suggest that this error is <  
16 4%, much smaller than the dilution uncertainty represented by our upper and lower limit  
17 estimates. The temperature of the plume was set at a constant value of 288.4 K, pressure of  
18 880 hPa, and relative humidity of 15.7% based on the observations of Akagi et al. (2012). The  
19 parcel was assumed to be emitted at 11:00 Pacific Standard Time (PST) and the model was  
20 integrated for 5 hours. The integration of the different terms of the continuity Equations 3-5  
21 were operator split for computational efficiency. The chemistry and mixing time steps were 1  
22 s for the first 10 minutes of model integration due to the rapid dilution and chemical changes  
23 during this period, and were 60 s thereafter. The aerosol thermodynamics, condensation, and  
24 coagulation time steps were 60 s throughout.

25 The initial and background concentrations for the gas-phase inorganic and NMOC species are  
26 in Table S3 of the Supplemental Material, and Table S4 gives the initial and background  
27 concentrations used for the aerosol species. Initial and background concentrations of trace  
28 gases and aerosols in the smoke were taken from observations of the Williams Fire (Akagi et  
29 al., 2012), where available. Emission ratios for other species were calculated using the  
30 literature reviews of Akagi et al. (2011) and Andreae and Merlet (2001). Other background  
31 concentrations were taken from runs of the GEOS-Chem model (Bey et al., 2001), run for our  
32 period as in Fischer et al. (2014).



1 The volatility distribution for the POA was taken from the wood smoke study of Grieshop et  
2 al. (2009a,b). Table 1 shows the POA total mass fractions used for wood smoke in Grieshop  
3 et al. (2009a) and the values used in this study for the Williams fire. At the measured  
4 temperature (288.4 K) and initial concentration of organic aerosol in the Williams fire smoke  
5 plume ( $849 \mu\text{g m}^{-3}$ ), the Grieshop et al. (2009a) POA volatility distribution implies that 81%  
6 of the total mass of SVOC species SVOC<sub>1</sub> to SVOC<sub>7</sub> is in the aerosol phase, leaving  $200 \mu\text{g}$   
7  $\text{m}^{-3}$  of SVOC species in the gas phase. Note that the May et al. (2013) POA volatility  
8 distribution (not shown in Table 1) is more volatile than Grieshop et al. (2009a), with 65% of  
9 the total mass of SVOC species SVOC<sub>1</sub> to SVOC<sub>7</sub> in the aerosol phase, leaving about  $460 \mu\text{g}$   
10  $\text{m}^{-3}$  of SVOC species in the gas phase.

11 However, Grieshop et al. (2009a) and May et al. (2013) were only able to measure species  
12 with a saturation mass concentration ( $C^*$ ) of  $10^4 \mu\text{g m}^{-3}$  or less. Furthermore, Akagi et al.  
13 (2011) provide emission factors for unidentified non-methane organic compounds (NMOCs)  
14 from savannah/grassland and chaparral fires, with unidentified NMOCs estimated to be equal  
15 in mass to the identified species. The savannah/grassland estimate is about twice as large as  
16 the chaparral estimate, as fewer species have been identified in chaparral fires. Here we use  
17 the savannah/grassland estimate to calculate an emission ratio of 0.195 g unidentified  
18 NMOC/g CO, but assign this value an uncertainty of ~50%, consistent with the lower  
19 chaparral estimate. This implies that there is about  $2000 \pm 1000 \mu\text{g m}^{-3}$  of unidentified NMOCs  
20 in the gas-phase of the smoke. So to be consistent with the EFs of Akagi et al. (2011) and the  
21 volatility distributions of Grieshop et al. (2009a) and May et al. (2013), there still needs to be  
22 another  $1500\text{--}1800 \mu\text{g m}^{-3}$  of unidentified NMOCs initially in the plume with  $C^* > 10^4 \mu\text{g m}^{-3}$   
23 which the techniques used by Grieshop et al. (2009) and May et al. (2013) would not have  
24 been able to measure. These remaining unidentified NMOCs were included as SVOC<sub>8</sub> ( $C^* =$   
25  $10^5 \mu\text{g m}^{-3}$ ), as shown in Table 1 and Tables S3 and S4 of the Supplemental Material. Below  
26 we also discuss sensitivity tests that were performed to see how the results change if the  
27 remaining unidentified NMOCs are considered as SVOC<sub>9</sub> ( $C^* = 10^6 \mu\text{g m}^{-3}$ ) instead, as well  
28 as for an increase or decrease of the estimated unidentified SVOC concentrations by 50%.

29 For all organic species, we assumed a constant  $\kappa = 0.04$ , corresponding to an O/C ratio of 0.25  
30 (Jimenez et al., 2009) that is typical of biomass burning organic aerosol (Donahue et al.,  
31 2011). Since the relative humidity in the Williams fire plume was very low, this assumption  
32 had little impact on our results.

1 The initial smoke aerosol size distribution was assumed to be a log-normal with a geometric  
2 mean diameter  $D_g$  of 0.10  $\mu\text{m}$  and a standard deviation  $\sigma$  of 1.9 (unitless) based on Reid and  
3 Hobbs (1998) for flaming combustion of Brazilian cerrado, which structurally is a similar mix  
4 of shrubs and grasses as in the Williams fire. The initial total number concentration of aerosol  
5 particles ( $2.34 \times 10^6$  particles  $\text{cm}^{-3}$ ) was calculated such that the initial total organic aerosol  
6 mass matched the  $\Delta\text{OA}/\Delta\text{CO}_2$  emission ratio from Akagi et al. (2012). The evolution of the  
7 aerosol size distribution with time was simulated by ASP v2.1 using a center-moving  
8 sectional size distribution with 10 bins, 8 bins for particles with volume-equivalent spherical  
9 diameters between 0.05 and 2.0  $\mu\text{m}$ , one for particles with diameters smaller than 0.05  $\mu\text{m}$ ,  
10 and one for particles with diameters greater than 2  $\mu\text{m}$ .

11 Photolysis rates were calculated offline using TUV v5.0 (Madronich and Flocke, 1998) as  
12 noted in Section 2.2 above. The smoke aerosols were assumed to dilute with time according to  
13 the three dilution rates derived above (see Figure 3). In the TUV simulations, we assumed no  
14 clouds and an initial AOD of 8.0 at 330 nm (consistent with the ASP v2.1 calculated initial  
15 extinction coefficient and the assumed plume thickness of 1 km), which decreases due to  
16 dilution assuming a background concentration of  $\sim 0$ . As noted above, we assumed a constant  
17 single scattering albedo of 0.9 based on Reid et al. (2005a). We also assumed initial plume  
18 and background concentrations of the trace gases  $\text{NO}_2$  (initial 295 ppbv, background 0 ppbv)  
19 and  $\text{SO}_2$  (initial 50.9 ppbv, background 0 ppbv). For the photolysis rate calculations only,  $\text{O}_3$   
20 was assumed to be 0 initially and increased after 15 minutes to a constant value of 100 ppbv  
21 to account for the observed formation of  $\text{O}_3$  within the smoke plume. The overhead ozone  
22 column was assumed to be 278 Dobson Units (DU), based on the average of values from the  
23 Ozone Monitoring Instrument (OMI) for 11/16/2009 (276 DU) and 11/18/2009 (280 DU)  
24 (accessed through [http://jwocky.gsfc.nasa.gov/teacher/ozone\\_overhead.html](http://jwocky.gsfc.nasa.gov/teacher/ozone_overhead.html) on June 2012,  
25 now at [http://ozoneaq.gsfc.nasa.gov/tools/ozonemap/ozone\\_overhead](http://ozoneaq.gsfc.nasa.gov/tools/ozonemap/ozone_overhead)). The surface albedo  
26 was assumed to be 0.035 based on the GEOS-Chem data file for the  $0.5^\circ \times 0.667^\circ$  North  
27 American grid for November 1985, which is in turn based on data from the Total Ozone  
28 Mapping Spectrometer (TOMS). Photolysis rates were calculated for three altitudes: just  
29 above the plume (i.e., at 2.1 km altitude), near the middle of the plume (1.6 km), and near the  
30 bottom of the plume (1.1 km). This, combined with the three dilution rates, gave nine  
31 estimates of photolysis rates versus time. The nine values for the  $\text{NO}_2$  photolysis rate ( $J_{\text{NO}_2}$ )  
32 were compared with the clear sky (no aerosol) case in Figure 4. In the middle of the plume

1 (1.6 km),  $J_{NO_2}$  was reduced from an initial clear-sky value of  $9 \times 10^{-3} \text{ s}^{-1}$  to an initial value of  
2  $2 \times 10^{-3} \text{ s}^{-1}$ . However, by 15 minutes after emission  $J_{NO_2}$  in the middle of the plume increased  
3 to  $6\text{-}8.5 \times 10^{-3} \text{ s}^{-1}$  depending on the dilution rate, showing that the plume reduced photolysis  
4 rates by 5-33% after the initial, rapid dilution of the plume.  $J_{NO_2}$  was slightly enhanced above  
5 the plume (initially  $1.1 \times 10^{-2} \text{ s}^{-1}$ ) over the clear sky value, and the photolysis rates were lowest  
6 in the bottom of the plume. As expected, the impact of the plume was larger for lower dilution  
7 rates, but the difference between the different dilution rates was largest for the bottom of the  
8 plume. Note that, while our assumption of a constant SSA is questionable as aerosol  
9 absorption is likely to change with both smoke age and with wavelength, our use of three  
10 dilution rates and three altitudes in the plume results in a wide range of photolysis rates used  
11 in this study, which can also account for uncertainties in the aerosol optical properties and  
12 other parameters used to calculate the photolysis rates.

## 13 **5.2 ASP Results with No Unidentified SVOC Chemistry**

14 We first ran ASP assuming the unidentified SVOCs emitted by the fire are unreactive.  
15 Deficiencies in these simulations provide information on what the average chemistry of the  
16 unidentified SVOCs needs to be in order to explain the observations.

17 Figure 5 shows the ASP v2.1 results and Akagi et al. (2012) observations for the enhancement  
18 ratios (EnR, mol/mol) of  $O_3$  and PAN in the Williams fire smoke plume versus time after  
19 emissions. The EnR is defined as the ratio of the enhancement of a species X within the  
20 smoke plume ( $\Delta X = C_x - C_x^a$ , Akagi et al., 2011) to the enhancement of a less reactive species,  
21 such as  $CO_2$  or  $CO$ . The choice of whether to use  $CO$  or  $CO_2$  in the denominator of the EnR  
22 was made on a species-by-species basis to match the choices made in Table 2 of Akagi et al.  
23 (2012), which were in turn chosen to minimize the impact of measurement and sampling  
24 errors on the EnRs. We can see that the range of dilution rates and photolysis rates simulated  
25 for this case capture the general rate of the secondary formation of  $O_3$  and PAN, but ASP v2.1  
26 appears to be overestimating the rate of formation of these compounds. This is in contrast to  
27 Alvarado and Prinn (2009), who found that ASP v1.0 underestimated the much faster  $O_3$   
28 formation in the Timbavati savannah fire smoke plume by about 50%.

29 The ASP v2.1 value for the best estimate dilution and photolysis case (i.e., the best-fit dilution  
30 combined with the middle of the plume photolysis rates, plotted as a solid black line in Figure

1 5) at 4.5 hours for  $\Delta\text{O}_3/\Delta\text{CO}$  is 0.116 mol/mol which is within the uncertainty associated with  
2 the average value measured for the Williams fire ( $0.095\pm 0.022$ ). This overestimate is similar  
3 to the positive bias (~25%) of the SAPRC-07 mechanism versus the EPA smog chamber  
4 results for low ROG/NO<sub>x</sub> (<20 ppb C/ppb N) ratios when aromatics are not part of the  
5 surrogate. As aromatics are a minor constituent in biomass burning smoke, and the ROG/NO<sub>x</sub>  
6 ratio for savannah/scrubland fires like the Williams fire (without including unidentified  
7 species) is ~10 ppb C/ppb N, we would expect the mechanism in ASP v2.1 to show a similar  
8 positive bias. ASP v2.1 predicts an “average” value of  $\Delta\text{PAN}/\Delta\text{CO}_2$  of  $8.4\times 10^{-4}$  at 4.5 hours  
9 downwind, 65% larger than the observed value of  $(5.10\pm 1.21)\times 10^{-4}$ .

10 Figure 6 shows the ASP v2.1 results and observations for  $\Delta\text{NO}_x/\Delta\text{CO}_2$  and  $\Delta\text{C}_2\text{H}_4/\Delta\text{CO}$   
11 versus time after emission. Figure 6a shows that the  $\Delta\text{NO}_x/\Delta\text{CO}_2$  values are correctly  
12 simulated by ASP v2.1, with the best estimate dilution and photolysis case EnR of  $3.4\times 10^{-4}$   
13 matching the observed value of  $4.6\pm 2.3\times 10^{-4}$  4 to 4.5 hours downwind. However, the  
14 observations show a faster rate of decay in the first two hours after emission than is seen in  
15 the model results. Figure 6b shows that the decay of C<sub>2</sub>H<sub>4</sub> is also well matched by the model  
16 results, suggesting that the modeled OH is similar to the actual OH concentrations. This can  
17 also be seen by comparing the modeled OH concentration for the best estimate dilution and  
18 photolysis case ( $5.3\times 10^6$  molecules cm<sup>-3</sup>) to that derived by Akagi et al. (2012) using the  
19 observed decay of C<sub>2</sub>H<sub>4</sub> ( $5.27\pm 0.97\times 10^6$  molecules cm<sup>-3</sup>). This is again in contrast with  
20 Alvarado and Prinn (2009), who found that ASP underestimated the observed OH radical  
21 concentrations for the Timbavati smoke plume ( $1.7\times 10^7$  molecules cm<sup>-3</sup>, Hobbs et al., 2003).

22 We can explore this contrast further by looking at the rate of loss of HONO in the smoke  
23 plume, shown in Figure 7. Note that unlike the previous figures, Figure 7 only shows the first  
24 hour after emission as the observations showed no detectable HONO further downwind. As  
25 noted in Section 1, to explain the underestimate of O<sub>3</sub> and OH in the Timbavati fire, Alvarado  
26 and Prinn (2009) posited that a heterogeneous reaction of NO<sub>2</sub> to make HONO and HNO<sub>3</sub> was  
27 taking place in that plume. However, the O<sub>3</sub> and OH results for the Williams fire show no  
28 evidence of this chemistry, and the HONO decay seen in Figure 7 also shows little evidence  
29 for a secondary source of HONO except for a few points within the first 12 minutes after  
30 emission that have more HONO than is predicted by the model. While explaining the  
31 discrepancy between the Williams and Timbavati results is beyond the scope of this paper, we  
32 note that the Timbavati fire took place closer to the equator (24°S versus 35°N), earlier in the

1 year (7 September versus 17 November) than the Williams fire, and that the relative humidity  
2 was higher as well (45.0% versus 15.7%). All of these differences would tend to increase  
3 photolysis rates and the formation of OH. In addition, the higher actinic flux and RH in  
4 Timbavati may have increased the speed of reactions for forming HONO from NO<sub>2</sub> that are  
5 not included in standard chemical mechanisms, either via aqueous chemistry (Jacob et al.,  
6 2000), sunlight-activated humic acid surfaces (Stemmler et al., 2006, 2007), or photo-excited  
7 NO<sub>2</sub> reacting with H<sub>2</sub>O (Ensberg et al., 2010). Though we find no evidence for secondary  
8 HONO production in the Williams Fire data, this does not preclude that some HONO was  
9 made, but remained below the AFTIR detection limit of 10 ppbv as the plume diluted.

10 Figure 8 shows the ASP results for two aldehydes, HCHO and glycoaldehyde (HCOCH<sub>2</sub>OH),  
11 and two organic acids, formic acid (HCOOH) and acetic acid (CH<sub>3</sub>COOH), in the Williams  
12 fire plume in terms of EnRs to CO. We can see that ASP generally underestimates the  
13 formation of these species. Part of this underestimate may be due to errors in the chemical  
14 mechanism for known precursor compounds, as was seen for HCHO in the smog chamber  
15 results, but neglecting the chemistry of the SVOCs and their ability to form these smaller  
16 organic compounds is also likely responsible for this underestimate.

17 Figure 9 shows the modeled OA enhancement ratios ( $\Delta\text{OA}/\Delta\text{CO}_2$ , g/g) at 4.5 hours  
18 downwind using the parameters listed in Table 2 in addition to the observed average OA  
19 enhancement ratio ( $2.83 \pm 1.08 \times 10^{-3}$ ) and the modeled OA enhancement ratio for the case  
20 where the chemistry of the unidentified SVOCs is not included ( $2.27 \times 10^{-3}$ ). When SVOC  
21 chemistry was not included, some of the original OA evaporated into the gas phase as the  
22 plume diluted, and as there was no chemistry to make these SVOC species less volatile, they  
23 stayed in the gas phase leading to a net decrease in  $\Delta\text{OA}/\Delta\text{CO}_2$  with time. Changing the gas-  
24 phase concentrations of the unidentified SVOC by  $\pm 50\%$  has a small impact ( $\sim 3\%$ ) on these  
25 results, but the match between the model and observation could be improved by using a less  
26 volatile POA distribution than that given by Grieshop et al. (2009a). However, the modeled  
27 decrease without SVOC chemistry is larger (but still within the error bars) than the decrease  
28 that was reported by Akagi et al. (2012). In addition, the assumption that the SVOCs do not  
29 react is unrealistic – as large multi-functional organic compounds, they should have a  
30 relatively fast reaction rate with OH (see Section 5.3 below). Thus in Sections 5.3 through 5.5  
31 below we test different, more realistic implementations for the chemistry of these SVOCs.

### 5.3 OH Reaction Rate and Fragmentation Probability of the Unidentified SVOCs

Here we evaluate the ability of the parameters from the original VBS paper of Robinson et al. (2007), a study of SOA formation in wood smoke by Grieshop et al. (2009a,b), and the implementation of the VBS scheme into WRF-Chem by Ahmadov et al. (2012) to simulate the observed evolution of OA in the Williams fire plume. Table 2 shows the values for the parameters in Reactions R3 and R4 that define these various SVOC mechanisms. Figure 9 shows that the SVOC mechanisms of Robinson et al. (2007) and Grieshop et al. (2009a,b) overestimated the OA downwind by a factor of 1.8 and 3.7, respectively. This is primarily due to their relatively large values for  $k_{OH}$ . For the Grieshop et al. (2009a,b) case, the overestimation is also partially due to the large increase in mass ( $\mu$ ) and decrease in volatility ( $n$ ) for each OH reaction. The OA formed using these mechanisms can be reduced by a further 25% if we assume the unidentified SVOCs are mainly the more volatile SVOC<sub>9</sub> ( $C^* = 10^6 \mu\text{g m}^{-3}$ ) instead of SVOC<sub>8</sub> ( $C^* = 10^5 \mu\text{g m}^{-3}$ ), but are fairly insensitive to errors in the POA volatility distribution. The scheme of Ahmadov et al. (2012), with  $k_{OH} = 10^{-11} \text{ cm}^3 \text{ molecule}^{-1} \text{ s}^{-1}$ , was consistent with the uncertainty in the observations, but slightly higher than the observed value ( $3.48 \times 10^{-3}$  versus the observed value of  $2.83 \pm 1.08 \times 10^{-3}$ ). One approach to further reduce the modeled OA would be to reduce  $k_{OH}$  even further. However, it seems unlikely that the average OH reaction rate of the unidentified SVOC species would be less than  $10^{-11} \text{ cm}^3 \text{ molecule}^{-1} \text{ s}^{-1}$ , as this is close to the reaction rate for large alkanes ( $k_{OH}(298\text{K}) = 1.1 \times 10^{-11} \text{ cm}^3 \text{ molecule}^{-1} \text{ s}^{-1}$ , Goliff et al, 2013) and the presence of other functional groups (double bonds, aldehydes) would be expected to result in even higher reaction rates. For example,  $\alpha$ -pinene has a  $k_{OH}(298\text{K})$  of  $5.0 \times 10^{-11} \text{ cm}^3 \text{ molecule}^{-1} \text{ s}^{-1}$  (Goliff et al., 2013), and other monoterpenes can have even faster reaction rates with OH. Thus, we think a more likely explanation for the remaining overestimate is that a substantial fraction of the SVOC and OH reactions resulted in the fragmentation of the primary SVOC into more volatile compounds, as in the 2D-VBS schemes of Jimenez et al. (2009) and Donahue et al. (2011).

Figure 9 shows that a  $k_{OH}$  of  $10^{-11} \text{ cm}^3 \text{ molecule}^{-1} \text{ s}^{-1}$  and a fragmentation probability of 50% (the “Half Fragmentation” case, see Table 2) provided a reasonably good match with the observed  $\Delta\text{OA}/\Delta\text{CO}_2$  4.5 hours downwind in the smoke plume ( $2.63 \times 10^{-3}$  versus the observed value of  $2.83 \pm 1.02 \times 10^{-3}$ ). Here we assumed that the SVOC fragmented into a small VOC and another, more volatile, SVOC, as in Reactions R3 and R4. While this is a relatively large

1 fragmentation probability, we note that it seems reasonable given the likely complex and  
2 multifunctional nature of the unidentified SVOCs in a biomass burning smoke plume.

3 This fragmentation of the SVOCs after reaction with OH could also help to explain the  
4 underestimate of aldehydes and organic acids seen in Section 5.2 when SVOC chemistry was  
5 neglected. For example, Figure 10 shows the ASP modeled EnR of acetic acid when we  
6 assumed that the VOC fragment produced in Reaction R4 is acetic acid. This provided a  
7 remarkably good match with the observed acetic acid formation, providing additional  
8 evidence to support the fragmentation hypothesis. While we are not claiming to have proven  
9 this is the source of the missing acetic acid, we note that the fragmentation hypothesis is thus  
10 consistent with the initial underestimate of the secondary formation of aldehydes and organic  
11 acids in ASP v2.1. In addition, there is some evidence from biomass burning plume  
12 observations that the formation of acetic acid and OA are inversely correlated with each other.  
13 In the Yucatan plume studied by Yokelson et al. (2009), a large amount of SOA was formed,  
14 but acetic acid did not increase downwind, while in the Williams Fire, acetic acid increased,  
15 but OA did not. Thus, the limited amount of relevant airborne data in BB plumes is so far  
16 consistent with the idea that the branching between functionalization and fragmentation in BB  
17 plumes is variable and future work should identify what environmental and combustion  
18 factors control the outcome.

19 An additional potential explanation for the SOA overestimate observed when the schemes of  
20 the Robinson et al. (2007), Grieshop et al. (2009a,b), and Ahmadov et al. (2012) were used is  
21 that the OA was becoming more viscous and “glassy” with time (i.e., the particles had a lower  
22 bulk diffusivity), thereby reducing the amount of quasi-liquid OA for SVOC compounds to  
23 dissolve into (e.g., Kidd et al., 2014; Zaveri et al., 2014). There has been some recent  
24 evidence for this process occurring in smoke plumes from biomass burning in the western US  
25 (A. Sedlacek, personal communication, March 2014). ASP v2.1 is not able to examine this  
26 possibility in detail, but we do note that while the formation of “glassy” OA would reduce  
27 SOA formation, it likely would not increase the formation of aldehydes or organic acids as in  
28 the fragmentation hypothesis.

#### 29 **5.4 HO<sub>x</sub> and NO<sub>x</sub> Chemistry of the Unidentified SVOCs**

30 Section 5.3 showed that an SVOC mechanism following Reaction R2 with a  $k_{OH}$  of  $10^{-11}$  cm<sup>3</sup>  
31 molecule<sup>-1</sup> s<sup>-1</sup> and a fragmentation probability  $\alpha$  of up to 0.5 (the “Half Fragmentation”

1 scheme in Table 2) could explain the observed evolution of OA in the Williams fire.  
2 However, neglecting the regeneration of HO<sub>x</sub> and reaction of the peroxy radical with NO, as  
3 in Reaction R2, can lead to substantial underestimates of OH in the concentrated smoke  
4 plumes. This is because including Reaction R2 in ASP leads to a loss of OH with no  
5 corresponding regeneration of HO<sub>2</sub>.

6 For example, Figure 11 shows that using the “Half Fragmentation” scheme reduced the ASP  
7 v2.1 estimates of the enhancement ratios of O<sub>3</sub> and PAN downwind by 24% and 23%,  
8 respectively (for the best estimate dilution and photolysis case, the black line in Figure 5),  
9 while Figure 12 shows that it increased the ASP v2.1 estimates of C<sub>2</sub>H<sub>4</sub> and NO<sub>x</sub> downwind  
10 by 33% and 151%, respectively. The “Half Fragmentation” O<sub>3</sub> and PAN estimates are more  
11 consistent with the observations – the overestimate of PAN seen with the unidentified SVOC  
12 chemistry neglected in Section 5.2 has disappeared – but the large overestimate of NO<sub>x</sub> (i.e.,  
13 underestimate of NO<sub>x</sub> loss in the plume presumably due to missing organic nitrogen  
14 formation) is a serious problem. While this underestimate of NO<sub>x</sub> loss reduces the amount of  
15 O<sub>3</sub> and PAN formed within five hours after emission, it would lead to large overestimates of  
16 the impact of biomass burning plumes on O<sub>3</sub> and PAN formation further downwind.

17 In addition, the chemistry of Reaction R2 is unrealistic, in that it implies a total loss of OH  
18 and no effect of the SVOC oxidation on NO<sub>x</sub>. One approach for addressing the first concern is  
19 to artificially regenerate the OH by simply adding it as an additional product to Reaction R2.  
20 While this makes sense as a “first do no harm” modeling approach to keep the gas-phase  
21 results the same regardless of the SVOC scheme, it is equally unrealistic, as it assumes that  
22 the SVOCs are oxidized without having any impact on NO<sub>x</sub> or HO<sub>x</sub>.

23 We prefer to approach this problem by recognizing that SVOCs are going to have impacts on  
24 the HO<sub>x</sub> and NO<sub>x</sub> radical budgets just like any other organic species, and that this chemistry  
25 can be approximated via Reactions R3 and R4. Including this more realistic, yet still  
26 simplified, chemistry allows ASP to simultaneously simulate the observed changes in OA and  
27 O<sub>3</sub> while still making reasonable, chemically plausible assumptions about the chemistry of the  
28 unidentified SVOCs emitted by the fire.

29 Our approach thus used the observations of OA, O<sub>3</sub>, PAN, NO<sub>x</sub>, and C<sub>2</sub>H<sub>4</sub> in the Williams fire  
30 as constraints on  $\beta$  and  $\delta$ , the amount of NO<sub>2</sub> and HO<sub>2</sub> produced in Reaction R4, respectively,  
31 while assuming that  $\chi=1$  throughout. For the Williams Fire, we know from the above results  
32 that we want the optimized SVOC chemistry to (a) increase O<sub>3</sub>, PAN, and OA formation as



1 little as possible, (b) increase the loss of  $\text{NO}_x$ , either through organic nitrate formation or  
2 increased OH concentrations, and (c) increase the OH concentration, thereby increasing  $\text{C}_2\text{H}_4$   
3 loss. We found that using the parameters for large alkanes from RACM2 ( $\delta = 0.63$  and  $\beta =$   
4  $0.74$ ) generally produced too much  $\text{O}_3$  and PAN and too little OH, but did a reasonable job for  
5  $\text{NO}_x$  loss. However, attempts to increase OH by increasing  $\delta$  led to too much  $\text{O}_3$  formation  
6 except for unrealistically low values of  $\beta$  ( $\sim 0.1$ ). Thus we set  $\delta = 0.6$  and reduced  $\beta$  to  $0.5$ ,  
7 implying that  $1.1 \text{ O}_3$  is formed per molecule of SVOC reacted. These parameters (arrived at  
8 by trial and error) appear to give the best balance of reducing modeled  $\text{NO}_x$  and  $\text{C}_2\text{H}_4$  mixing  
9 ratios while minimizing the increase in  $\text{O}_3$ , PAN, and OA. The following section discusses  
10 the ASP v2.1 model results for the Williams fire smoke plume using these parameters in  
11 detail. Note that while slightly different, more precise parameters might provide a slightly  
12 better match with observation, our goal here is not to derive exact best-fit parameters, but  
13 rather to roughly classify the average chemistry of the SVOCs in the Williams fire smoke  
14 plume, both for modeling this fire and for future comparisons with other smoke plumes.

## 15 **5.5 Results with Optimized SVOC Chemistry**

16 Figure 9 shows the  $\Delta\text{OA}/\Delta\text{CO}_2$  4.5 hours downwind in the smoke plume using the optimized  
17 SVOC chemistry discussed in Section 5.4. For the best estimate dilution and photolysis model  
18 case (i.e., the solid black line in Figure 5),  $\Delta\text{OA}/\Delta\text{CO}_2$  is  $2.75 \times 10^{-3} \text{ (g/g)}$ , very close to the  
19 observed value of  $2.83 \pm 1.02 \times 10^{-3}$ . As in Section 5.2, changing the gas-phase concentrations  
20 of the unidentified SVOC by  $\pm 50\%$  has a small impact ( $\sim 3\%$ ) on these results, as does  
21 assuming that the unidentified SVOCs are mainly the more volatile  $\text{SVOC}_9$  ( $C^* = 10^6 \mu\text{g m}^{-3}$ )  
22 instead of  $\text{SVOC}_8$  ( $C^* = 10^5 \mu\text{g m}^{-3}$ ). However, this result is still sensitive to the POA  
23 volatility distribution – for example, moving all the mass in  $\text{SVOC}_3$  ( $C^* = 1 \mu\text{g m}^{-3}$ ) to  
24  $\text{SVOC}_7$  ( $C^* = 10^4 \mu\text{g m}^{-3}$ ) decreases the modeled  $\Delta\text{OA}/\Delta\text{CO}_2$  downwind by 12% for this case.

25 Figure 13 shows the enhancement ratios of  $\text{O}_3$  and PAN for the optimized SVOC chemistry,  
26 and Figure 14 shows the results for  $\text{NO}_x$  and  $\text{C}_2\text{H}_4$ . The  $\text{O}_3$  results are very similar to those  
27 from Section 5.2 (where SVOC chemistry was not included in the model), while the PAN  
28 results are slightly lower (and closer to the observed values) than in that case. For the best  
29 estimate dilution and photolysis model case  $\Delta\text{O}_3/\Delta\text{CO}$  is  $0.119$  at 4.5 hours downwind, about  
30 25% larger than the observed value of  $0.095 \pm 0.022$ , while the  $\Delta\text{PAN}/\Delta\text{CO}_2$  is now  $7.56 \times 10^{-4}$   
31 at 4.5 hours downwind, about 48% larger than the observed value of  $(5.10 \pm 1.21) \times 10^{-4}$ .

1 However, the O<sub>3</sub> and PAN values are reasonably close given the uncertainties in the  
2 concentrations and in the estimated smoke ages for the observations.

3 The NO<sub>x</sub> results were much improved from the “half frag” case in Section 5.4, with the best  
4 estimate dilution and photolysis case  $\Delta\text{NO}_x/\Delta\text{CO}_2$  of  $1.6\times 10^{-4}$  being below the mean observed  
5 value of  $4.6\pm 2.3\times 10^{-4}$ , but consistent with the error bars of the individual samples as shown in  
6 Figure 14. We could attempt to get a closer match by increasing  $\beta$ , but at the cost of increases  
7 in the modeled O<sub>3</sub>, PAN, and OA formation. The decay of C<sub>2</sub>H<sub>4</sub> is also better modeled than in  
8 the Half Fragmentation case, suggesting the model OH is also improved. The modeled OH  
9 concentration for the best estimate dilution and photolysis case is now  $5.3\times 10^6$  molecules cm<sup>-3</sup>  
10 <sup>3</sup>, matching the observed value of  $5.27\pm 0.97\times 10^6$  molecules cm<sup>-3</sup>.

## 11 **6 Conclusions**

12 We have used version 2.1 of the ASP model, which includes extensive updates to the gas-  
13 phase chemistry and SOA formation modules, to simulate the near-source chemistry within  
14 the smoke plume from the Williams fire, as sampled by Akagi et al. (2012). We find that the  
15 assumptions made about the chemistry of the unidentified SVOCs emitted by the fire have a  
16 large impact on the simulated secondary formation of O<sub>3</sub>, PAN, and OA within the plume. We  
17 showed that reasonable assumptions about the chemistry of the unidentified SVOCs can  
18 successfully simulate the observations within the uncertainties of the measurements, the  
19 estimated smoke ages of the samples, the plume dilution rate, and the vertical location of the  
20 samples in the plume. For the Williams fire, these assumptions were: (1) a reaction rate  
21 constant with OH of  $\sim 10^{-11}$  cm<sup>3</sup>/s; (2) a significant fraction (up to  $\sim 50\%$ ) of the RO<sub>2</sub> + NO  
22 reaction resulted in fragmentation, rather than functionalization; (3)  $\sim 1.1$  molecules of O<sub>3</sub>  
23 were formed for every molecule of SVOC that reacts; and (4) 60% of the OH that reacted  
24 with the SVOC was regenerated as HO<sub>2</sub> by the RO<sub>2</sub> + NO reaction, which implied (5) that  
25 50% of the NO that reacted with the SVOC peroxy radicals was lost, likely due to organic  
26 nitrate formation. However, this chemistry still overestimates PAN formation downwind by  
27 about 50%, suggesting the need for further refinements to the chemistry and estimated  
28 emission rates of PAN precursors like acetaldehyde. Furthermore, these specific, quantitative  
29 results only apply to the Williams fire analyzed in this paper. Further analysis of other smoke  
30 plume observations is needed to determine how these parameters vary between individual  
31 smoke plumes.

1 The method used in this study can provide a way of classifying different smoke plume  
2 observations in terms of the average chemistry of their unidentified SVOCs. Similar studies of  
3 other young biomass burning plumes would allow us to see how the chemistry of the  
4 unidentified SVOCs varies with combustion efficiency, fuel type, and other combustion and  
5 environmental parameters, providing an additional constraint on the reactivities of the  
6 unidentified SVOCs. These constraints could then provide more insight into the formation of  
7 O<sub>3</sub>, PAN, and OA in young biomass burning smoke plumes and serve as the basis of  
8 parameterizing this process for regional or global scale models. Future field experiments,  
9 focused on quasi-Lagrangian sampling of biomass burning smoke plumes, should ideally also  
10 provide data beyond that available for the Williams Fire that will increase our understanding  
11 of the chemistry of these plumes. These field experiments should include (a) observations of  
12 changes in particle size distribution to test model simulations of condensational growth,  
13 coagulation, and new particle formation; (b) observations of a larger suite of NO<sub>y</sub> species,  
14 such as HNO<sub>3(g)</sub>, peroxy nitrates, and alkyl nitrates, for use in studying and constraining the  
15 transformations of reactive nitrogen; (c) direct measurements of photolysis rates within the  
16 smoke plumes; (d) measurements of organic aerosol volatility, viscosity, and mixing state  
17 with black carbon and inorganic aerosols; and (e) more detailed measurements of the  
18 currently unidentified organic species present in the smoke plumes, including acetaldehyde,  
19 an important PAN precursor.

## 20 **Acknowledgements**

21 The authors thank the anonymous reviewers and Dr. Manish Kumar Shrivastava of Pacific  
22 Northwest National Laboratory (PNNL) for their helpful comments. This modeling work was  
23 funded by NSF grant number AGS-1144165 to MJA and CRL of Atmospheric and  
24 Environmental Research (AER) and RY of the University of Montana. Original sampling of  
25 the Williams fire was funded primarily by the Strategic Environmental Research and  
26 Development Program (SERDP) projects SI-1648 and SI-1649 and partially by NSF grants  
27 ATM-0513055 and ATM-0936321. The California Institute of Technology contributions were  
28 partially funded through Dreyfus Award EP-11-117 to JSC.

29

## 1 **References**

- 2 Ahmadov, R., McKeen, S. A., Robinson, A. L., Bahreini, R., Middlebrook, A. M., de Gouw,  
3 J. A., Meagher, J., Hsie, E.-Y., Edgerton, E., Shaw, S., and Trainer, M.: A volatility basis set  
4 model for summertime secondary organic aerosols over the eastern United States in 2006, *J.*  
5 *Geophys. Res.*, 117, 2156–2202, 2012.
- 6 Akagi, S. K., Yokelson, R. J., Wiedinmyer, C., Alvarado, M. J., Reid, J. S., Karl, T., Crouse,  
7 J. D., and Wennberg, P. O.: Emission factors for open and domestic biomass burning for use  
8 in atmospheric models, *Atmos. Chem. Phys.*, 11, 4039–4072, 2011.
- 9 Akagi, S. K., Craven, J. S., Taylor, J. W., McMeeking, G. R., Yokelson, R. J., Burling, I. R.,  
10 Urbanski, S. P., Wold, C. E., Seinfeld, J. H., Coe, H., Alvarado, M. J., and Weise, D. R.:  
11 Evolution of trace gases and particles emitted by a chaparral fire in California, *Atmos. Chem.*  
12 *Phys.*, 12, 1397–1421, 2012.
- 13 Akagi, S. K., Yokelson, R. J., Burling, I. R., Meinardi, S., Simpson, I., Blake, D. R.,  
14 McMeeking, G. R., Sullivan, A., Lee, T., Kreidenweis, S., Urbanski, S., Reardon, J.,  
15 Griffith, D. W. T., Johnson, T. J., and Weise, D. R.: Measurements of reactive trace gases and  
16 variable O<sub>3</sub> formation rates in some South Carolina biomass burning plumes, *Atmos. Chem.*  
17 *Phys.*, 13, 1141–1165, doi:10.5194/acp-13-1141-2013, 2013.
- 18 Allan, J. D., Delia, A. E., Coe, H., Bower, K. N., Alfarra, M. R., Jimenez, J. L., Middlebrook,  
19 A. M., Drewnick, F., Onasch, T. B., Canagaratna, M. R., Jayne, J. T., and Workshop, D. R.: A  
20 generalized method for the extraction of chemically resolved mass spectra from Aerodyne  
21 aerosol mass spectrometer data, *J. Aerosol Sci.*, 35, 909–922, 2004.
- 22 Alvarado, M. J.: Formation of Ozone and Growth of Aerosols in Young Smoke Plumes from  
23 Biomass Burning, Ph.D. Thesis, Massachusetts Institute of Technology, Cambridge, MA,  
24 USA, 324 pp., available at [http://globalchange.mit.edu/files/document/Alvarado\\_PhD\\_08.pdf](http://globalchange.mit.edu/files/document/Alvarado_PhD_08.pdf)  
25 (last accessed December 11, 2014), 2008.
- 26 Alvarado, M. J., and Prinn, R. G.: Formation of Ozone and Growth of Aerosols in Young  
27 Smoke Plumes from Biomass Burning, Part 1: Lagrangian Parcel Studies, *J. Geophys. Res.*,  
28 114, D09306, doi:10.1029/2008JD011144, 2009.

1 Alvarado, M. J., Wang, C., and Prinn, R. G.: Formation of Ozone and Growth of Aerosols in  
2 Young Smoke Plumes from Biomass Burning, Part 2: 3D Eulerian Studies, *J. Geophys. Res.*,  
3 114, D09307, doi:10.1029/2008JD011186, 2009.

4 Alvarado, M. J., Logan, J. A., Mao, J., Apel, E., Riemer, D., Blake, D., Cohen, R. C., Min,  
5 K.-E., Perring, A. E., Browne, E. C., Wooldridge, P. J., Diskin, G. S., Sachse, G. W.,  
6 Fuelberg, H., Sessions, W. R., Harrigan, D. L., Huey, G., Liao, J., Case-Hanks, A., Jimenez, J.  
7 L., Cubison, M. J., Vay, S. A., Weinheimer, A. J., Knapp, D. J., Montzka, D. D., Flocke, F.  
8 M., Pollack, I. B., Wennberg, P. O., Kurten, A., Crounse, J., St. Clair, J. M., Wisthaler, A.,  
9 Mikoviny, T., Yantosca, R. M., Carouge, C. C., and Le Sager, P.: Nitrogen oxides and PAN  
10 in plumes from boreal fires during ARCTAS-B and their impact on ozone: an integrated  
11 analysis of aircraft and satellite observations, *Atmos. Chem. Phys.*, 10, 9739–9760, 2010.

12 Alvarado, M. J., Cady-Pereira, K. E., Xiao, Y., Millet, D. B., and Payne, V. H.: Emission  
13 Ratios for Ammonia and Formic Acid and Observations of Peroxy Acetyl Nitrate (PAN) in  
14 Biomass Burning Smoke As Seen By the Tropospheric Emission Spectrometer (TES),  
15 *Atmosphere*, 2, 633–654, doi:10.3390/atmos2040633, 2011.

16 Andreae, M. O., Anderson, B. E., Blake, D. R., Bradshaw, J. D. Collins, J. E., Gregory, G. L.,  
17 Sachse, G. W., and Shipham M. C.: Influence of plumes from biomass burning on  
18 atmospheric chemistry over the equatorial and tropical South Atlantic during CITE 3, *J.*  
19 *Geophys. Res.*, 99(D6), 12793–12808, doi:[10.1029/94JD00263](https://doi.org/10.1029/94JD00263), 1994.

20 Andreae, M. O., and Merlet, P.: Emission of trace gases and aerosols from biomass burning,  
21 *Global Biogeochem. Cycles*, 15, 955–966, 2001.

22 Arnold, S. R., Emmons, L. K., Monks, S. A., Law, K. S., Ridley, D. A., Turquety, S.,  
23 Tilmes, S., Thomas, J. L., Bouarar, I., Flemming, J., Huijnen, V., Mao, J., Duncan, B. N.,  
24 Steenrod, S., Yoshida, Y., Langner, J., and Long, Y.: Biomass burning influence on high  
25 latitude tropospheric ozone and reactive nitrogen in summer 2008: a multi-model analysis  
26 based on POLMIP simulations, *Atmos. Chem. Phys. Discuss.*, 14, 24573–24621,  
27 doi:10.5194/acpd-14-24573-2014, 2014.

28 Atkinson, R., Baulch, D. L., Cox, R. A., Crowley, J. N., Hampson, R. F., Hynes, R. G.,  
29 Jenkin, M. E., Rossi, M. J., and Troe, J.: Evaluated kinetic and photochemical data for  
30 atmospheric chemistry: Volume I - gas phase reactions of O<sub>x</sub>, HO<sub>x</sub>, NO<sub>x</sub> and SO<sub>x</sub> species,  
31 *Atmos. Chem. Phys.*, 4, 1461–1738, doi:10.5194/acp-4-1461-2004, 2004.

1 Baylon, P., Jaffe, D. A., Wigder, N. L., Gao, H., & Hee, J.: Ozone enhancement in Western  
2 US wildfire plumes at the Mt. Bachelor Observatory: The Role of NO<sub>x</sub>, Atmospheric  
3 Environment, in press, 2014.

4 Beswick, K. M., Gallagher, M. W., Webb, A. R., Norton, E. G., and Perry, F.: Application of  
5 the Aventech AIMMS20AQ airborne probe for turbulence measurements during the  
6 Convective Storm Initiation Project, *Atmos. Chem. Phys.*, 8, 5449–5463, doi:10.5194/acp-8-  
7 5449-2008, 2008.

8 Bey, I., Jacob, D. J., Yantosca, R. M., Logan, J. A., Field, B. D., Fiore, A. M., Li, Q., Liu, H.  
9 Y., Mickley, L. J., and Schultz, M. G.: Global modeling of tropospheric chemistry with  
10 assimilated meteorology: Model description and evaluation, *J. Geophys. Res.* 106, D19  
11 23073–23095, 2001.

12 Bloss, C., Wagner, V., Jenkin, M. E., Volkamer, R., Bloss, W. J., Lee, J. D., Heard, D. E.,  
13 Wirtz, K., Martin-Reviejo, M., Rea, G., Wenger, J. C., and Pilling, M. J.: Development of a  
14 detailed chemical mechanism (MCMv3.1) for the atmospheric oxidation of aromatic  
15 hydrocarbons, *Atmos. Chem. Phys.*, 5, 641–664, doi:10.5194/acp-5-641-2005, 2005.

16 Bowman, F. M., and Seinfeld, J. H.: Fundamental basis of incremental reactivities of organics  
17 in ozone formation in VOC/NO<sub>x</sub> mixtures, *Atmos. Environ.*, 28(20), 3359–3368, 1994a.

18 Bowman, F. M., and Seinfeld, J. H. Ozone productivity of atmospheric organics, *J. Geophys.*  
19 *Res.*, 99(D3), 5309–5324, 1994b.

20 Canagaratna, M. R., Jayne, J. T., Jimenez, J. L., Allan, J. D., Alfarra, M. R., Zhang, Q.,  
21 Onasch, T. B., Drewnick, F., Coe, H., Middlebrook, A., Delia, A., Williams, L. R., Trimborn,  
22 A. M., Northway, M. J., DeCarlo, P. F., Kolb, C. E., Davidovits, P., and Worsnop, D. R.:  
23 Chemical and microphysical characterization of ambient aerosols with the Aerodyne aerosol  
24 mass spectrometer, edited by: Viggiano, A., *Mass Spectrom. Rev.*, 26, 185–222, 2007.

25 Capes, G., Johnson, B., McFiggans, G., Williams, P. I., Haywood, J., and Coe, H.: Aging of  
26 biomass burning aerosols over West Africa: Aircraft measurements of chemical composition,  
27 microphysical properties, and emission ratios, *J. Geophys. Res.*, 113, D00C15,  
28 doi:[10.1029/2008JD009845](https://doi.org/10.1029/2008JD009845), 2008.

29 Carter, W. P.: Development of ozone reactivity scales for volatile organic compounds, *Air*  
30 *and Waste*, 44(7), 881–899, 1994.

1 Carter, W., Luo, D., Malkina, I., and Pierce, J.: Environmental chamber studies of  
2 atmospheric reactivities of volatile organic compounds: Effects of varying ROG surrogate and  
3 NO<sub>x</sub>, Tech. rep., Final Report to Coordinating Research Council, Inc., Project ME-9,  
4 California Air Resources Board, Contract A032-0692, and South Coast Air Quality  
5 Management District, Contract C91323, available at [http://www.cert.ucr.edu/  
6 carter/absts.htm#rct2rpt](http://www.cert.ucr.edu/carter/absts.htm#rct2rpt), 1995.

7 Carter, W. P.: Documentation of the SAPRC-99 chemical mechanism for VOC reactivity  
8 assessment, Tech. rep., Draft report to the California Air Resources Board, Contracts 92-329  
9 and 95-308, 2000.

10 Carter, W. P., Cocker, I., David, R., Fitz, D. R., Malkina, I. L., Bumiller, K., Sauer, C. G.,  
11 Pisano, J. T., Bufalino, C., and Song, C.: A new environmental chamber for evaluation of gas-  
12 phase chemical mechanisms and secondary aerosol formation, *Atmospheric Environment*, 39,  
13 7768–7788, 2005.

14 Carter, W. P. L.: Mechanism and updated ozone reactivity scales, Report to the California Air  
15 Resources Board, Contracts No. 03-318, 06-408, and 07-730, January 27, 2010.

16 Christian, T., Kleiss, B., Yokelson, R., Holzinger, R., Crutzen, P., Hao, W., Saharjo, B., and  
17 Ward, D.: Comprehensive laboratory measurements of biomass-burning emissions: 1.  
18 Emissions from Indonesian, African, and other fuels, *J. Geophys. Res.*, 108, 4719-4731,  
19 doi:10.1029/2003JD003704, 2003.

20 Crouse, J. D., Paulot, F., Kjaergaard, H. G., and Wennberg, P.O.: Peroxy radical  
21 isomerization in the oxidation of isoprene, *Phys. Chem. Chem. Phys.*, 13, 13607–13613,  
22 2011.

23 Crouse, J. D., Knap, H. C., Ørnsø, K. B., Jørgensen, S., Paulot, F., Kjaergaard, H. G., and  
24 Wennberg, P. O.: Atmospheric Fate of Methacrolein. 1. Peroxy Radical Isomerization  
25 Following Addition of OH and O<sub>2</sub>, *J. Phys. Chem. A*, 116, 5756–5762, 2012.

26 Crutzen, P. J., and Andreae, M. O.: Biomass burning in the tropics: Impact on atmospheric  
27 chemistry and biogeochemical cycles, *Science*, 250, 1669—1678, 1990.

28 Donahue, N. M., Epstein, S. A., Pandis, S. N., and Robinson, A. L.: A two-dimensional  
29 volatility basis set: 1. Organic-aerosol mixing thermodynamics, *Atmos. Chem. Phys.*, 11,  
30 3303–3318, doi:10.5194/acp-11-3303-2011, 2011.

1 Drewnick, F., Schwab, J. J., Hogrefe, O., Peters, S., Husain, L., Diamond, D., Weber, R., and  
2 Demerjian, K. L.: Intercomparison and evaluation of four semi-continuous PM<sub>2.5</sub> sulfate  
3 instruments, *Atmos. Environ.*, 37, 3335–3350, 2003.

4 Drewnick, F., Hings, S. S., DeCarlo, P., Jayne, J. T., Gonin, M., Fuhrer, K., Weimer, S.,  
5 Jimenez, J. L., Demerjian, K. L., Borrmann, S., and Worsnop, D. R.: A new Time-of-Flight  
6 Aerosol Mass Spectrometer (TOF-AMS) – instrument description and first field deployment,  
7 *Aerosol Sci. Tech.*, 39, 637–658, 2005.

8 Dzepina, K., Volkamer, R. M., Madronich, S., Tulet, P., Ulbrich, I. M., Zhang, Q., Cappa, C.  
9 D., Ziemann, P. J., and Jimenez, J. L.: Evaluation of recently-proposed secondary organic  
10 aerosol models for a case study in Mexico City, *Atmos. Chem. Phys.*, 9, 5681–5709,  
11 doi:10.5194/acp-9-5681-2009, 2009.

12 Ensberg, J. J., Carreras-Sospedra, M., and Dabdub, D.: Impacts of electronically photo-  
13 excited NO<sub>2</sub> on air pollution in the South Coast Air Basin of California, *Atmos. Chem. Phys.*,  
14 10, 1171–1181, doi:10.5194/acp-10-1171-2010, 2010.

15 Fischer, E. V., Jaffe, D. A., Reidmiller, D. R., and Jaeglé, L.: Meteorological controls on  
16 observed peroxyacetyl nitrate at Mount Bachelor during the spring of 2008, *J. Geophys.*  
17 *Res.*, 115, D03302, doi:[10.1029/2009JD012776](https://doi.org/10.1029/2009JD012776), 2010.

18 Fischer, E. V., Jacob, D. J., Yantosca, R. M., Sulprizio, M. P., Millet, D. B., Mao, J.,  
19 Paulot, F., Singh, H. B., Roiger, A., Ries, L., Talbot, R.W., Dzepina, K., and  
20 Pandey Deolal, S.: Atmospheric peroxyacetyl nitrate (PAN): a global budget and source  
21 attribution, *Atmos. Chem. Phys.*, 14, 2679–2698, doi:10.5194/acp-14-2679-2014, 2014.

22 Fountoukis, C. and Nenes, A.: ISORROPIA II: a computationally efficient thermodynamic  
23 equilibrium model for K<sup>+</sup>–Ca<sup>2+</sup>–Mg<sup>2+</sup>–NH<sub>4</sub><sup>+</sup>–Na<sup>+</sup>–SO<sub>4</sub><sup>2-</sup>–NO<sub>3</sub><sup>-</sup>–Cl<sup>-</sup>–H<sub>2</sub>O aerosols, *Atmos.*  
24 *Chem. Phys.*, 7, 4639–4659, doi:10.5194/acp-7-4639-2007, 2007.

25 Goliff, W.S., Stockwell, W. R., and Lawson, C. V.: The regional atmospheric chemistry  
26 mechanism, version 2, *Atmos. Environ.*, 68, 174–185, 2013.

27 Goode, J. G., Yokelson, R. J., Ward, D. E., Susott, R. A., Babbitt, R. E., Davies, M. A., and  
28 Hao, W. M.: Measurements of excess O<sub>3</sub>, CO<sub>2</sub>, CO, CH<sub>4</sub>, C<sub>2</sub>H<sub>4</sub>, C<sub>2</sub>H<sub>2</sub>, HCN, NO, NH<sub>3</sub>,  
29 HCOOH, CH<sub>3</sub>COOH, HCHO and CH<sub>3</sub>OH in 1997 Alaskan biomass burning plumes by  
30 airborne fourier transform infrared spectroscopy (AFTIR), *J. Geophys. Res.*, 105, 22,147–  
31 22,166, 2000.



1 Grieshop, A. P., Logue, J. M., Donahue, N.M., and Robinson A. L.: Laboratory investigation  
2 of photochemical oxidation of organic aerosol from wood fires 1: measurement and  
3 simulation of organic aerosol evolution, *Atmos. Chem. Phys.*, 9, 1263–1277, doi:10.5194/acp-  
4 9-1263-2009, 2009a.

5 Grieshop, A. P., Donahue, N. M., and Robinson, A. L.: Laboratory investigation of  
6 photochemical oxidation of organic aerosol from wood fires 2: analysis of aerosol mass  
7 spectrometer data, *Atmos. Chem. Phys.*, 9, 2227–2240, doi:10.5194/acp-9-2227-2009, 2009b.

8 Griffin, R. J., Nguyen, K., Dabdub, K. D., and Seinfeld, J. H.: A coupled hydrophobic-  
9 hydrophilic model for predicting secondary organic aerosol formation, *J. Atmos. Chem.*, 44,  
10 171–190, 2003.

11 Griffin, R. J., Dabdub, D., and Seinfeld, J. H.: Development and initial evaluation of a  
12 dynamic species-resolved model for the gas phase chemistry and size-resolved gas/particle  
13 partitioning associated with secondary organic aerosol formation, *J. Geophys. Res.*, 110,  
14 D05304, doi:10.1029/2004JD005219, 2005.

15 Heilman, W. E., Liu, Y., Urbanski, S., Kovalev, V., Mickler, R.: Wildland fire emissions,  
16 carbon, and climate: Plume rise, atmospheric transport, and chemistry processes, *For. Ecol.*  
17 *Manage.*, 317, 70-79, doi: 10.1016/j.foreco.2013.02.001, 2014,  
18 <http://www.treesearch.fs.fed.us/pubs/45645>.

19 Hennigan, C. J., Miracolo, M. A., Engelhart, G. J., May, A. A., Presto, A. A., Lee, T.,  
20 Sullivan, A. P., McMeeking, G. R., Coe, H., Wold, C. E., Hao, W.-M., Gilman, J. B., Kuster,  
21 W. C., de Gouw, J., Schichtel, B. A., Collett Jr., J. L., Kreidenweis, S. M., and Robinson, A.  
22 L.: Chemical and physical transformations of organic aerosol from the photo-oxidation of  
23 open biomass burning emissions in an environmental chamber, *Atmos. Chem. Phys.*, 11,  
24 7669–7686, doi:10.5194/acp-11-7669-2011, 2011.

25 Heringa, M. F., DeCarlo, P. F., Chirico, R., Tritscher, T., Dommen, J., Weingartner, E.,  
26 Richter, R., Wehrle, G., Prevot, A. S. H., and Baltensperger, U.: Investigations of primary and  
27 secondary particulate matter of different wood combustion appliances with a high-resolution  
28 time-of-flight aerosol mass spectrometer, *Atmos. Chem. Phys.*, 11, 5945–5957,  
29 doi:10.5194/acp-11-5945-2011, 2011.

1 Hobbs, P. V., Sinha, P., Yokelson, R. J., Christian, T. J., Blake, D. R., Gao, S., Kirchstetter,  
2 T. W., Novakov, T. and Pilewskie, P.: Evolution of gases and particles from a savanna fire in  
3 South Africa, *J. Geophys. Res.*, 108, 8485-8504, doi:[10.1029/2002JD002352](https://doi.org/10.1029/2002JD002352), 2003.

4 Holmes, C. D., Prather, M. J., and Vinken, G. C. M.: The climate impact of ship NO<sub>x</sub>  
5 emissions: an improved estimate accounting for plume chemistry, *Atmos. Chem. Phys.*, 14,  
6 6801–6812, doi:10.5194/acp-14-6801-2014, 2014.

7 Huffman, J. A., Jayne, J. T., Drewnick, F., Aiken, A. C., Onasch, T., Worsnop, D. R., and  
8 Jimenez, J. L.: Design, modeling, optimization, and experimental tests of a particle beam  
9 width probe for the aerodyne aerosol mass spectrometer, *Aerosol Sci. Technol.*, 39, 1143–  
10 1163, 2005.

11 Jacob, D., Wofsy, S., Bakwin, P., Fan, S.-M., Harriss, R., Talbot, R., Bradshaw, J., Sandholm,  
12 S., Singh, H., Browell, E.V. Gregory, G., Sachse, G., Shipham, M., Blake, D., and Fitzjarrald,  
13 D.: Summertime photochemistry of the troposphere at high northern latitudes, *J. Geophys.*  
14 *Res.*, 97(D15), 16421–16431, 1992.

15 Jacob, D. J.: Heterogeneous chemistry and tropospheric ozone, *Atmos. Environ.*, 34, 2131–  
16 2159, 2000.

17 Jacobson, M. Z.: Development and application of a new air pollution modeling system - II.  
18 Aerosol module structure and design, *Atmos. Environ.*, 31, 131–144, 1997.

19 Jacobson, M. Z.: Analysis of aerosol interactions with numerical techniques for solving  
20 coagulation, nucleation, condensation, dissolution, and reversible chemistry among multiple  
21 size distributions, *J. Geophys. Res.*, 107, 4366-4388, doi:10.1029/2001JD002044, 2002.

22 Jacobson, M. Z.: *Fundamentals of Atmospheric Modeling*, 2nd ed., Cambridge University  
23 Press, 2005.

24 Jaffe, D. A., and Wigder, N. L.: Ozone production from wildfires: A critical review,  
25 *Atmospheric Environment*, 51, 1–10, 2012.

26 Jaffe, D. A., Wigder, N., Downey, N., Pfister, G., Boynard, A., and Reid, S. B.: Impact of  
27 wildfires on ozone exceptional events in the western US, *Environ. Sci. Tech.*, 47(19), 11065–  
28 11072, 2013.

1 Jenkin, M. E., Saunders, S. M., and Pilling, M. J.: The tropospheric degradation of volatile  
2 organic compounds: a protocol for mechanism development, *Atmos. Environ.*, 31(1), 81–104,  
3 ISSN 1352-2310, DOI: 10.1016/S1352-2310(96)00105-7, 1997.

4 Jenkin, M. E., Saunders, S. M., Wagner, V., and Pilling, M. J.: Protocol for the development  
5 of the Master Chemical Mechanism, MCM v3 (Part B): tropospheric degradation of aromatic  
6 volatile organic compounds, *Atmos. Chem. Phys.*, 3, 181–193, doi:10.5194/acp-3-181-2003,  
7 2003.

8 Jiang, X., Wiedinmyer, C., and Carlton, A. G.: Aerosols from fires: An examination of the  
9 effects on ozone photochemistry in the Western United States, *Environ. Sci. and Technol.*,  
10 46 (21), 11878-11886, 2012.

11 Jimenez, J. L., Canagaratna, M. R., Donahue, N. M., Prevot, A. S. H., Zhang, Q., Kroll, J. H.,  
12 DeCarlo, P. F., Allan, J. D., Coe, H., Ng, N. L., Aiken, A. C., Docherty, K. S., Ulbrich, I. M.,  
13 Grieshop, A. P., Robinson, A. L., Duplissy, J., Smith, J. D., Wilson, K. R., Lanz, V. A.,  
14 Hueglin, C., Sun, Y. L., Tian, J., Laaksonen, A., Raatikainen, T., Rautiainen, J., Vaattovaara,  
15 P., Ehn, M., Kulmala, M., Tomlinson, J. M., Collins, D. R., Cubison, M. J., Dunlea, E. J.,  
16 Huffman, J. A., Onasch, T. B., Alfarra, M. R., Williams, P. I., Bower, K., Kondo, Y.,  
17 Schneider, J., Drewnick, F., Borrmann, S., Weimer, S., Demerjian, K., Salcedo, D., Cottrell,  
18 L., Griffin, R., Takami, A., Miyoshi, T, Hatakeyama, S., Shimono, A., Sun, J. Y., Zhang, Y.  
19 M., Dzepina, K., Kimmel, J. R., Sueper, D., Jayne, J. T., Herndon, S. C., Trimborn, A. M.,  
20 Williams, L. R., Wood, E. C., Middlebrook, A. M., Kolb, C. E., Baltensperger, U., and  
21 Worsnop, D. R.: Evolution of Organic Aerosols in the Atmosphere, *Science*, 326,1525–1529,  
22 2009.

23 Jost, C., Trentmann, J., Sprung, D., Andreae, M. O., McQuaid, J. B., and Barjat, H.: Trace gas  
24 chemistry in a young biomass burning plume over Namibia: Observations and model  
25 simulations, *J. Geophys. Res.*, 108 , 8482-8494, doi:10.1029/2002JD002431, 2003.

26 Kidd, C., Perraud, V., Wingen, L. M., and Finlayson-Pitts, B. J.: Integrating phase and  
27 composition of secondary organic aerosol from the ozonolysis of  $\alpha$ -pinene, *PNAS*, 111(21),  
28 7552–7557, doi:10.1073/pnas.1322558111, 2014.

29 Kusik, C., and Meissner, H.: Electrolyte activity coefficients in inorganic processing, in  
30 *Fundamental Aspects of Hydrometallurgical Processes*, AIChE Symposium Series, edited by  
31 T. Chapman, L. Taularides, G. Hubred, and R. Wellek, pp. 14–20, AIChE, New York, 1978.

1 Lapina, K., Honrath, R., Owen, R. C., Val Martin, M., and Pfister, G.: Evidence of significant  
2 large-scale impacts of boreal fires on ozone levels in the midlatitude Northern Hemisphere  
3 free troposphere, *Geophys. Res. Lett.*, 33, L10815, doi: 10.1029/2006GL025878, 2006.

4 Madronich, S., and Flocke, S.: The role of solar radiation in atmospheric chemistry.  
5 *Handbook of Environmental Chemistry*, P. Boule, Ed., Springer, 1-26, 1998.

6 Mason, S. A., Field, R. J., Yokelson, R. J., Kochivar, M. A., Tinsley, M. R., Ward, D. W. and  
7 Hao, W. M.: Complex effects arising in smoke plume simulations due to the inclusion of  
8 direct emissions of oxygenated organic species from biomass combustion, *J. Geophys. Res.*,  
9 106, 12,527–12,539, 2001.

10 Mason, S. A., Trentmann, J., Winterrath, T., Yokelson, R. J., Christian, T. J., Carlson, L. J.,  
11 Warner, T. R., Wolfe, L. C., and Andreae, M. O.: Intercomparison of two box models of the  
12 chemical evolution in biomass-burning smoke plumes, *J. Atmos. Chem.*, 55, 273–297,  
13 doi:10.1007/s10874-006-9039-5, 2006.

14 Mauzerall, D. L., Logan, J. A., Jacob, D. J., Anderson, B. E., Blake, D. R., Bradshaw, J. D.,  
15 Heikes, B., Sachse, G. W., Singh, H., and Talbot, B.: Photochemistry in biomass burning  
16 plumes and implications for tropospheric ozone over the tropical South Atlantic, *J. Geophys.*  
17 *Res.* 103, D7, 8401–8423, 1998.

18 Nenes, A., Pandis, S. N., and Pilinis, C.: ISORROPIA: A new thermodynamic equilibrium  
19 model for multiphase multicomponent inorganic aerosols, *Aquatic Geochemistry*, 4, 123–152,  
20 1998.

21 Pankow, J. F.: An absorption model of gas/particle partitioning of organic compounds in the  
22 atmosphere, *Atmos. Environ.*, 28, 185–188, 1994a.

23 Pankow, J. F.: An absorption model of the gas/aerosol partitioning involved in the formation  
24 of secondary organic aerosol, *Atmos. Environ.*, 28, 189–193, 1994b.

25 Parrington, M., Palmer, P. I., Lewis, A. C., Lee, J. D., Rickard, A. R., Di Carlo, P., Taylor, J.  
26 W., Hopkins, J. R., Punjabi, S., Oram, D. E., Forster, G., Aruffo, E., Moller, S. J., Bauguitte,  
27 S. J.-B., Allan, J. D., Coe, H., and Leigh, R. J.: Ozone photochemistry in boreal biomass  
28 burning plumes, *Atmos. Chem. Phys.*, 13, 7321–7341, doi:10.5194/acp-13-7321-2013, 2013.

1 Paulot, F., Crounse, J. D., Kjaergaard, H. G., Kroll, J. H., Seinfeld, J. H., and Wennberg, P.  
2 O.: Isoprene photooxidation: new insights into the production of acids and organic nitrates,  
3 *Atmos. Chem. Phys.*, 9, 1479–1501, 2009a.

4 Paulot, F., Kurten, A., St Clair, J. M., Seinfeld, J. H., and Wennberg, P.O.: Unexpected  
5 Epoxide Formation in the Gas-Phase Photooxidation of Isoprene, *Science*, 325, 730–733,  
6 2009b.

7 Petters, M. D., and Kreidenweis, S. M.: A single parameter representation of hygroscopic  
8 growth and cloud condensation nucleus activity, *Atmos. Chem. Phys.*, 7, 1961–1971,  
9 doi:10.5194/acp-7-1961-2007, 2007.

10 Pfister, G., Emmons, L. K., Hess, P. G., Honrath, R., Lamarque, J. F., Val Martin, M., Owen,  
11 R. C., Avery, M. A., Browell, E. V., Holloway, J. S., Nedelec, P., Purvis, R., Ryerson, R. B.,  
12 Sachse, G. W., and Schlager, H.: Ozone production from the 2004 North American boreal  
13 fires, *J. Geophys. Res.*, 111, D24S07, doi:10.1029/2006JD007695, 2006.

14 Pun, B. K., Griffin, R. J., Seigneur, C., and Seinfeld, J. H.: Secondary organic aerosol, 2,  
15 Thermodynamic model for Gas/Particle partitioning of molecular constituents, *J. Geophys.*  
16 *Res.*, 107, 4333-4347, doi:10.1029/2001JD000542, 2002.

17 Radke, L. F., Hegg, D. A., Hobbs, P. V., Nance, J. D., Lyons, J. H., Laursen, K. K., Weiss, R.  
18 E., Riggan, P. J., and Ward, D. E.: Particulate and trace gas emissions from large biomass  
19 fires in North America, *Global biomass burning – Atmospheric, climatic, and biospheric*  
20 *implications*, MIT Press, Cambridge, MA, 209–224, 1991.

21 Reid, J. S., and Hobbs, P. V.: Physical and optical properties of young smoke from individual  
22 biomass fires in Brazil, *J. Geophys. Res.*, 103, 32,013–32,030, 1998.

23 Reid, J. S., Eck, T., Christopher, S., Koppmann, R., Dubovik, O., Eleuterio, D., Holben, B.,  
24 Reid, E. A., and Zhang, J.: A review of biomass burning emissions Part III: Intensive optical  
25 properties of biomass burning particles, *Atmos. Chem. Phys.*, 5, 827–849, 2005a.

26 Reid, J. S., Koppmann, R., Eck, T., and Eleuterio, D.: A review of biomass burning emissions  
27 Part II: Intensive physical properties of biomass burning particles, *Atmos. Chem. Phys.*, 5,  
28 799–825, 2005b.

1 Resch, T.: A framework for modeling suspended multicomponent particulate systems with  
2 applications to atmospheric aerosols., Ph.D. thesis, Massachusetts Institute of Technology,  
3 1995.

4 Robinson, A. L., Donahue, N. M., Shrivastava, M. K., Weitkamp, E. A., Sage, A. M.,  
5 Grieshop, A. P., Lane, T. E., Pierce, J. R., and Pandis, S. N.: Rethinking Organic Aerosols:  
6 Semivolatile Emissions and Photochemical Aging, *Science*, 315, 1259–1262, 2007.

7 Sander, S. P., Abbatt, J., Barker, J. R., Burkholder, J. B., Friedl, R. R., Golden, D. M., Huie,  
8 R. E., Kolb, C. E., Kurylo, M. J., Moortgat, G. K., Orkin, V. L., and Wine, P. H.: "Chemical  
9 Kinetics and Photochemical Data for Use in Atmospheric Studies, Evaluation No. 17," JPL  
10 Publication 10-6, Jet Propulsion Laboratory, Pasadena, <http://jpldataeval.jpl.nasa.gov>, 2011.

11 Saunders, S. M., Jenkin, M. E., Derwent, R. G., and Pilling, M. J.: Protocol for the  
12 development of the Master Chemical Mechanism, MCM v3 (Part A): tropospheric  
13 degradation of non-aromatic volatile organic compound, *Atmos. Chem. Phys.*, 3, 161–180,  
14 2003.

15 Seinfeld, J. H., and Pandis, S. N.: *Atmospheric Chemistry and Physics*, John Wiley and Sons,  
16 New York, NY, 1998.

17 Shrivastava, M.K.B, Zelenyuk, A., Imre, D., Easter, R. C., Jr., Beranek, J., Zaveri, R. A., and  
18 Fast, J. D.: Implications of Low Volatility SOA and Gas-Phase Fragmentation Reactions on  
19 SOA Loadings and their Spatial and Temporal Evolution in the Atmosphere. *J. Geophys.*  
20 *Res.*, 118, 3328-3342. doi:10.1002/jgrd.50160, 2013.

21 Singh, H. B., Cai, C., Kaduwela, A., Weinheimer, A., and Wisthaler, A.: Interactions of fire  
22 emissions and urban pollution over California: Ozone formation and air quality simulations.  
23 *Atmos. Environ.*, 56, 45–51, 2012.

24 Sommers, W. T., Loehman, R. A. Hardy, C. C.: Wildland fire emissions, carbon, and climate:  
25 Science overview and knowledge needs. *For. Ecol. Manage.*, 317, 1-8, doi:  
26 10.1016/j.foreco.2013.12.014, 2014, <http://www.treesearch.fs.fed.us/pubs/45726>.

27 Steele, H. D.: Investigations of cloud altering effects of atmospheric aerosols using a new  
28 mixed eulerian-lagrangian aerosol model, Ph.D. thesis, Massachusetts Institute of  
29 Technology, ([http://web.mit.edu/cgcs/www/MIT\\_CGCS\\_Rpt74.pdf](http://web.mit.edu/cgcs/www/MIT_CGCS_Rpt74.pdf)), 2004.

1 Stemmler, K., Ammann, M., Donders, C., Kleffmann, J., and George, C.: Photosensitized  
2 reduction of nitrogen dioxide on humic acid as a source of nitrous acid, *Nature*, 440, 195–198,  
3 doi:10.1038/nature04603, 2006.

4 Stemmler, K., Ndour, M., Elshorbany, Y., Kleffmann, J., D’Anna, B., George, C., Bohn, B.,  
5 and Ammann, M.: Light induced conversion of nitrogen dioxide into nitrous acid on  
6 submicron humic acid aerosol, *Atmos. Chem. Phys.*, 7, 4237–4248, 2007.

7 Stokes, R. H., and Robinson, R. A.: Interactions in aqueous nonelectrolyte solutions. I.  
8 Solute-Solvent Equilibria, *J. Phys. Chem.*, 70, 2126–2130, 1966.

9 Sudo, K., and Akimoto, H.: Global source attribution of tropospheric ozone: Long-range  
10 transport from various source regions, *J. Geophys. Res.*, 112, D12302,  
11 doi:[10.1029/2006JD007992](https://doi.org/10.1029/2006JD007992), 2007.

12 Trentmann, J., Andreae, M. O., and Graf, H.-F.: Chemical processes in a young biomass-  
13 burning plume, *J. Geophys. Res.*, 108, 4705-4714, doi:10.1029/2003JD003732, 2003.

14 Trentmann, J., Yokelson, R. J., Hobbs, P. V., Winterrath, T., Christian, T. J., Andreae, M. O.,  
15 and Mason, S. A.: An analysis of the chemical processes in the smoke plume from a savannah  
16 fire, *J. Geophys. Res.*, 110, D12301, doi:10.1029/2004JD005628, 2005.

17 Vakkari, V., Kerminen, V., Beukes, J.P., Tiitta, P., van Zyl, P.G., Josipovic, M., Venter, A.D.,  
18 Jaars, K., Worsnop, D.R., Kulmala M., and Laakso, L.: Rapid changes in biomass burning  
19 aerosols by atmospheric oxidation, *Geophys. Res. Lett.*, 41, 2644–2651,  
20 doi:[10.1002/2014GL059396](https://doi.org/10.1002/2014GL059396), 2014.

21 Val Martin, M., Honrath, R. E., Owen, R. C., Pfister, G., Fialho, P., and Barata, F.:  
22 Significant enhancements of nitrogen oxides, ozone and aerosol black carbon in the North  
23 Atlantic lower free troposphere resulting from North American boreal wildfires, *J. Geophys.*  
24 *Res.*, 111, D23S60, doi:10.1029/2006JD007530, 2006.

25 van der Werf, G. R., Randerson, J. T., Giglio, L., Collatz, G. J., Mu, M., Kasibhatla, P. S.,  
26 Morton, D. C., DeFries, R. S., Jin, Y., and van Leeuwen, T. T.: Global fire emissions and the  
27 contribution of deforestation, savanna, forest, agricultural, and peat fires (1997–2009), *Atmos.*  
28 *Chem. Phys.*, 10, 11707-11735, doi:10.5194/acp-10-11707-2010, 2010.

1 Vinken, G. C. M., Boersma, K. F., Jacob, D. J., and Meijer, E. W.: Accounting for non-linear  
2 chemistry of ship plumes in the GEOS-Chem global chemistry transport model, *Atmos.*  
3 *Chem. Phys.*, 11, 11707–11722, doi:10.5194/acp-11-11707-2011, 2011.

4 Warneke, C., Roberts, J. M., Veres, P., Gilman, J., Kuster, W. C., Burling, I., Yokelson, R. J.,  
5 and de Gouw, J. A.: VOC identification and inter-comparison from laboratory biomass  
6 burning using PTR-MS and PIT-MS, *Int. J. Mass Spectrom. Ion Proc.*, 303, 6–14, doi:  
7 10.1016/j.ijms.2010.12.002, 2011.

8 Wilson, J. C., Lafleur, B. G., Hilbert, H., Seebaugh, W. R., Fox, J., Gesler, D.W., Brock, C.  
9 A., Huebert, B. J., and Mullen, J.: Function and performance of a low turbulence inlet for  
10 sampling supermicron particles from aircraft platforms, *Aerosol Sci. Tech.*, 38, 790–802,  
11 2004.

12 Yarwood, G., Rao, S., Yocke, M., and Whitten, G. Z.: Updates to the carbon bond chemical  
13 mechanism: CB05, RT-04-00675, Prepared for Deborah Luecken, U.S. Environmental  
14 Protection Agency Research Triangle Park, NC 27703, ENVIRON, available at  
15 [http://www.camx.com/publ/pdfs/cb05\\_final\\_report\\_120805.pdf](http://www.camx.com/publ/pdfs/cb05_final_report_120805.pdf), 2005.

16 Yokelson, R. J., Goode, J. G., Ward, D. E., Susott, R. A., Babbitt, R. E., Wade, D. D.,  
17 Bertschi, I., Griffith, D. W. T., and Hao, W. M.: Emissions of formaldehyde, acetic acid,  
18 methanol, and other trace gases from biomass fires in North Carolina measured by airborne  
19 Fourier transform infrared spectroscopy, *J. Geophys. Res.*, 104, 30109–30126,  
20 doi:10.1029/1999JD900817, 1999.

21 Yokelson, R. J., Bertschi, I. T., Christian, T. J., Hobbs, P. V., Ward, D. E., and Hao, W. M.:  
22 Trace gas measurements in nascent, aged, and cloud-processed smoke from African savanna  
23 fires by airborne fourier transform infrared spectroscopy (AFTIR), *J. Geophys. Res.*, 108,  
24 8478-8491, doi:10.1029/2002JD002322, 2003.

25 Yokelson, R. J., Urbanski, S. P., Atlas, E. L., Toohey, D. W., Alvarado, E. C., Crouse, J. D.,  
26 Wennberg, P. O., Fisher, M. E., Wold, C. E., Campos, T. L., Adachi, K., Buseck, P. R., and  
27 Hao, W. M.: Emissions from forest fires near Mexico City, *Atmos. Chem. Phys.*, 7, 5569–  
28 5584, doi:10.5194/acp-7-5569-2007, 2007.

29 Yokelson, R. J., Crouse, J. D., DeCarlo, P. F., Karl, T., Urbanski, S., Atlas, E., Campos, T.,  
30 Shinozuka, Y., Kapustin, V., Clarke, A. D., Weinheimer, A., Knapp, D. J., Montzka, D. D.,  
31 Holloway, J., Weibring, P., Flocke, F., Zheng, W., Toohey, D., Wennberg, P. O.,



- 1 Wiedinmyer, C., Mauldin, L., Fried, A., Richter, D., Walega, J., Jimenez, J. L., Adachi, K.,  
2 Buseck, P. R., Hall, S. R., and Shetter, R.: Emissions from biomass burning in the Yucatan,  
3 *Atmos. Chem. Phys.*, 9, 5785–5812, 2009.
- 4 Zaveri, R. A., Easter, R. C., Shilling, J. E., and Seinfeld, J. H.: Modeling kinetic partitioning  
5 of secondary organic aerosol and size distribution dynamics: representing effects of volatility,  
6 phase state, and particle-phase reaction, *Atmos. Chem. Phys.*, 14, 5153–5181,  
7 doi:10.5194/acp-14-5153-2014, 2014.
- 8 Zdanovskii, A. B.: New methods for calculating solubilities of electrolytes in multi-  
9 component systems, *Zhur. Fiz. Kim.*, 22, 1475–1485, 1948.
- 10 Zhang, L., Jacob, D. J., Yue, X., Downey, N. V., Wood, D. A., and Blewitt, D.: Sources  
11 contributing to background surface ozone in the US Intermountain West, *Atmos. Chem.*  
12 *Phys.*, 14(11), 5295–5309, 2014.
- 13
- 14

1 Table 1. Definition of SVOC species following Grieshop et al. (2009a).

Species	$C^*$ ( $\mu\text{g m}^{-3}$ @ 300 K)	$\Delta H_{vap}$ ( $\text{kJ mol}^{-1}$ )	MW ( $\text{g mol}^{-1}$ )	POA volatility distributions <sup>a</sup>	
				Grieshop et al. (2009a)	This study <sup>b</sup>
SVOC <sub>1</sub>	$10^{-2}$	77	524	0	0
SVOC <sub>2</sub>	$10^{-1}$	73	479	0	0
SVOC <sub>3</sub>	$10^0$	69	434	0.1	0.038
SVOC <sub>4</sub>	$10^1$	65	389	0.14	0.0532
SVOC <sub>5</sub>	$10^2$	61	344	0.33	0.1254
SVOC <sub>6</sub>	$10^3$	57	299	0.33	0.1254
SVOC <sub>7</sub>	$10^4$	54	254	0.1	0.038
SVOC <sub>8</sub>	$10^5$	50	208	0	0.62
SVOC <sub>9</sub>	$10^6$	46	163	0	0

2 <sup>a</sup>Relative mass emissions in each volatility bin.

3 <sup>b</sup>Where the relative amounts of SVOC<sub>*i*</sub> (*i*=1 to 7) are kept as in Grieshop et al. (2009a), but  
 4 additional organic mass is added to SVOC<sub>8</sub> to account for the unidentified NMOC mass  
 5 reported by Akagi et al. (2011).

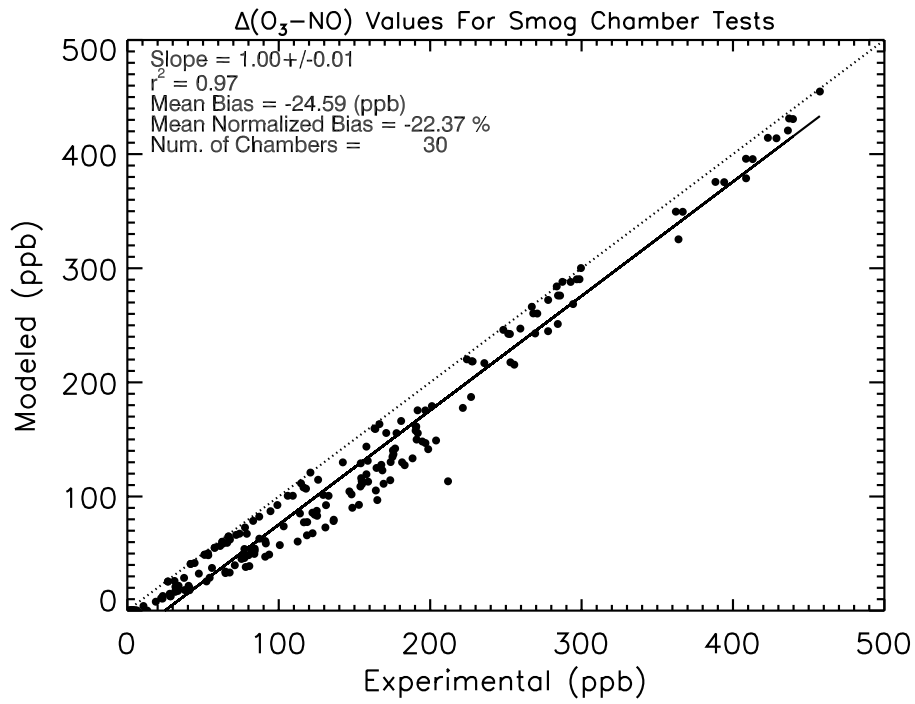
6

- 1 Table 2. SVOC chemistry parameters in the mechanisms studied here. See Reactions R3 and  
 2 R4 for definitions of the parameters.

Mechanism	$k_{OH} \times 10^{11}$ ( $\text{cm}^3 \text{ molecule}^{-1} \text{ s}^{-1}$ )	$\mu$	$n$	$\alpha$	$\chi$	$\beta$	$\delta$
Grieshop et al. (2009)	2.0	1.4	2	0	0	0	0
Robinson et al. (2007)	4.0	1.075	1	0	0	0	0
Ahmadov et al. (2012)	1.0	1.075	1	0	0	0	0
Half Fragmentation	1.0	1.075	1	.5	0	0	0
Optimized SVOC Chemistry	1.0	1.075	1	.5	1	.5	.6

3 .

1

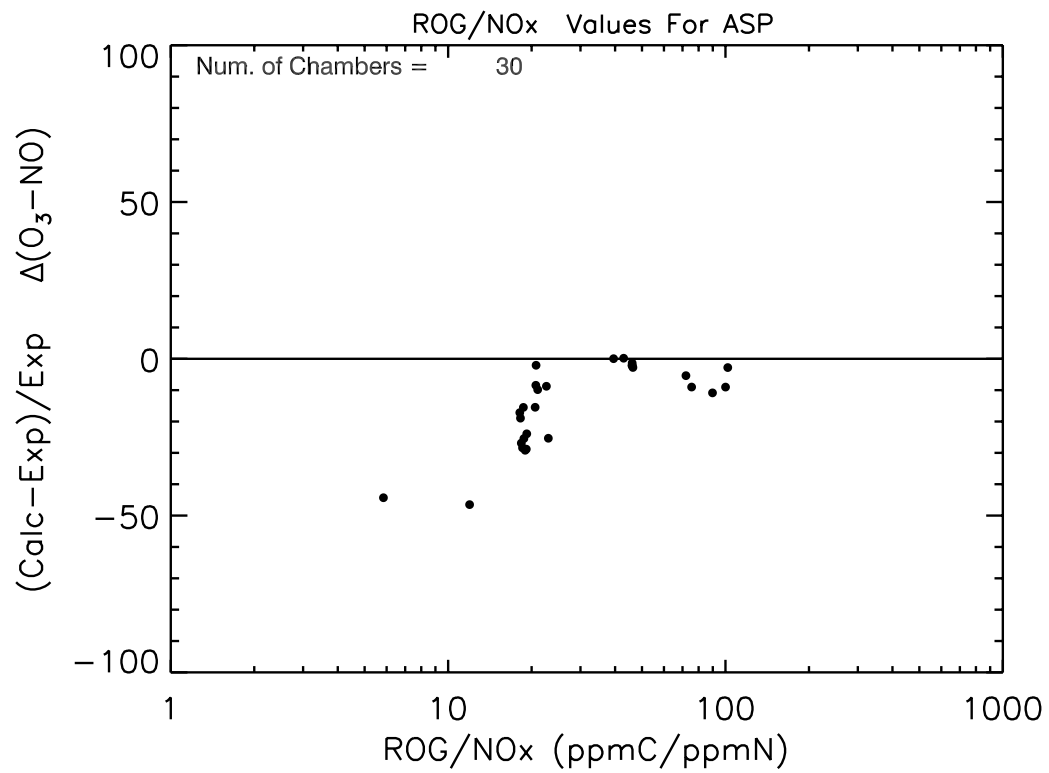


2

3

4 Figure 1. ASP calculated hourly values of  $\Delta([\text{O}_3] - [\text{NO}]) \equiv ([\text{O}_3]_{\text{final}} - [\text{NO}]_{\text{final}}) - ([\text{O}_3]_{\text{initial}} -$   
5  $[\text{NO}]_{\text{initial}})$  versus the values measured in the EPA chamber of Carter et al. (2005) for 30 “full  
6 surrogate” experiments. Note that all time points for the 30 chamber experiments are plotted,  
7 not just the final values.

8



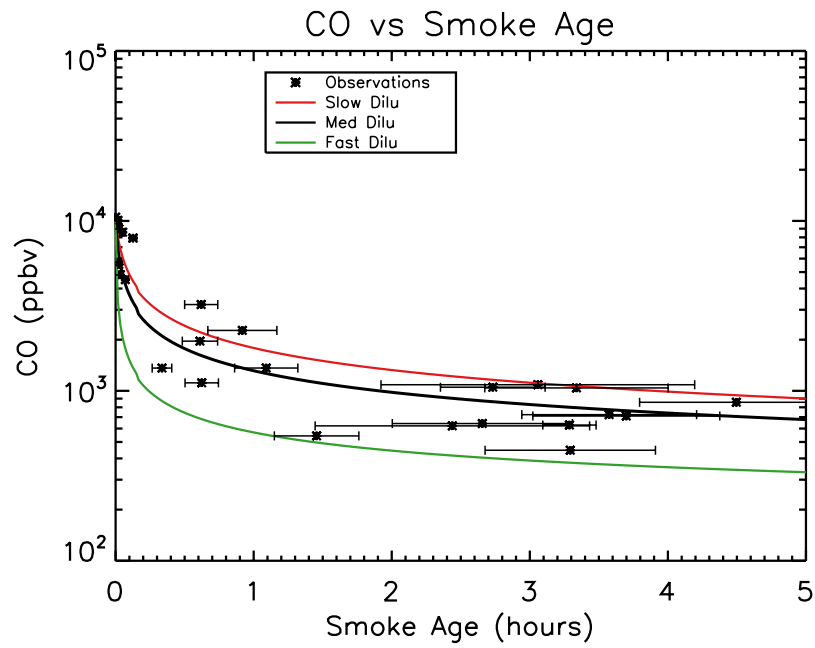
1

2

3 Figure 2. Percentage bias in final  $\Delta([\text{O}_3] - [\text{NO}])$  versus the initial ratio of reactive organic  
 4 gases (ROG) to  $\text{NO}_x$  (ppm C/ppm N) for the chamber experiments.

5

6

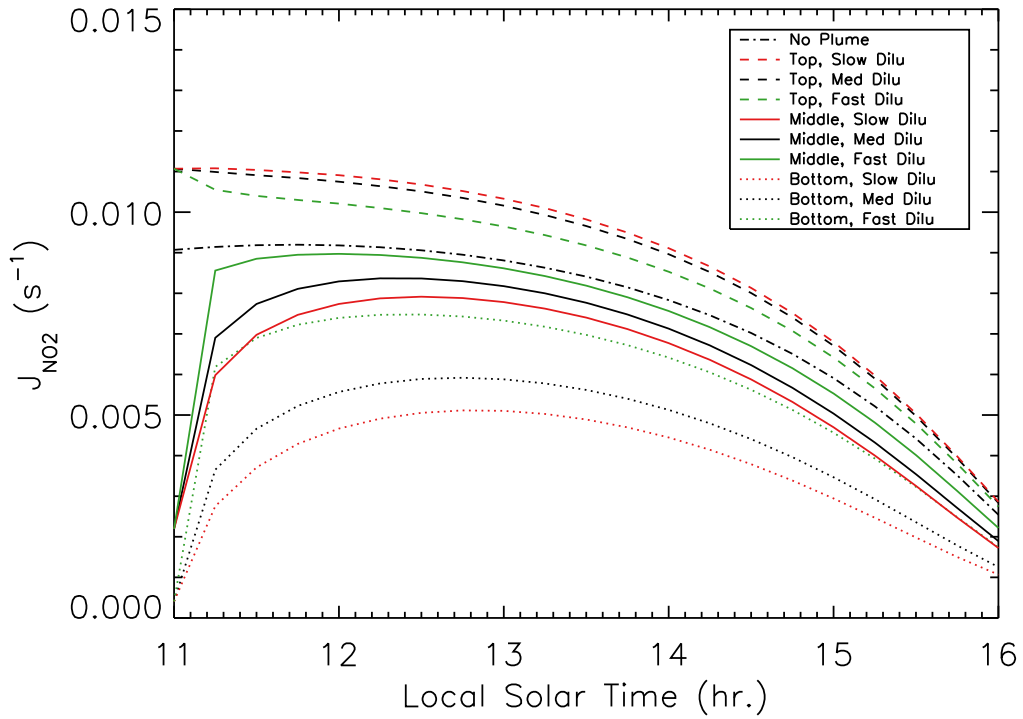


1

2

3 Figure 3. CO mixing ratio (ppbv) versus smoke age. Red, black, and green are for the slow,  
 4 best-fit (medium), and fast plume dilution rates. Asterisks are the measured mixing ratios,  
 5 with the horizontal error bars showing the uncertainty in the estimated age, which is much  
 6 larger than the uncertainty in the CO mixing ratio.

7

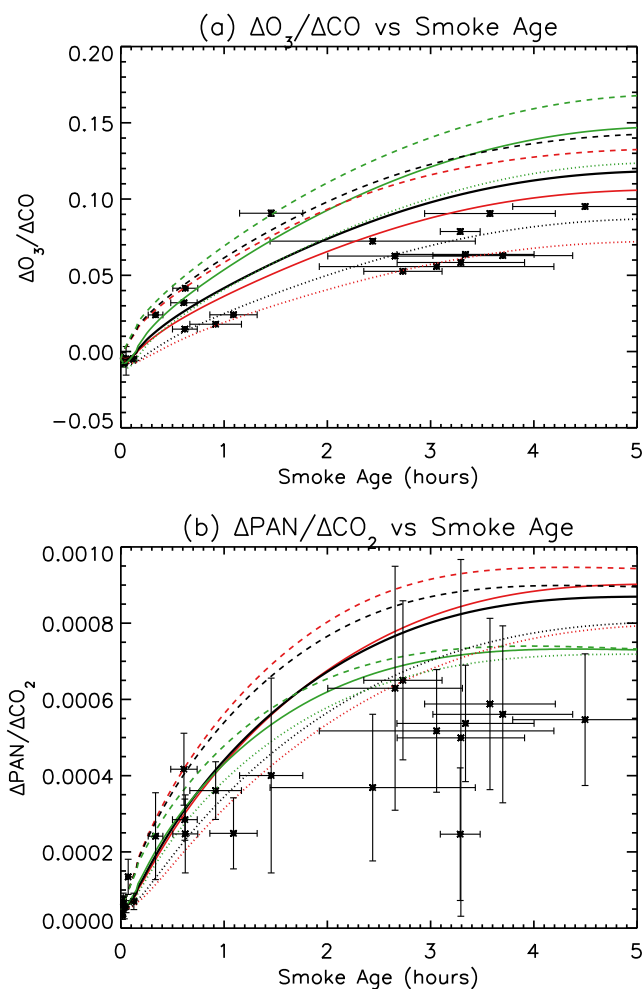


1

2

3 Figure 4. NO<sub>2</sub> photolysis rates (s<sup>-1</sup>) versus local time. Red, black, and green are for the slow,  
 4 best-fit (medium), and fast plume dilution rates. Dashed lines are for photolysis rates above  
 5 the plume, solid lines are for the middle of the plume, and dotted lines are for the bottom of  
 6 the plume, as described in the text. The black dot-dashed line is the clear-sky (no plume)  
 7 photolysis rate.

8

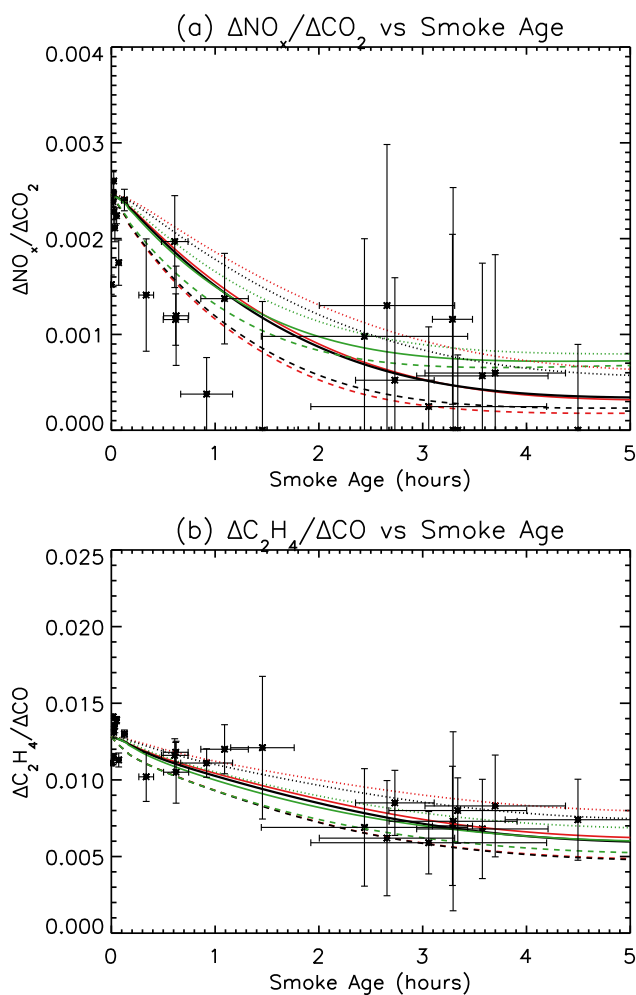


1

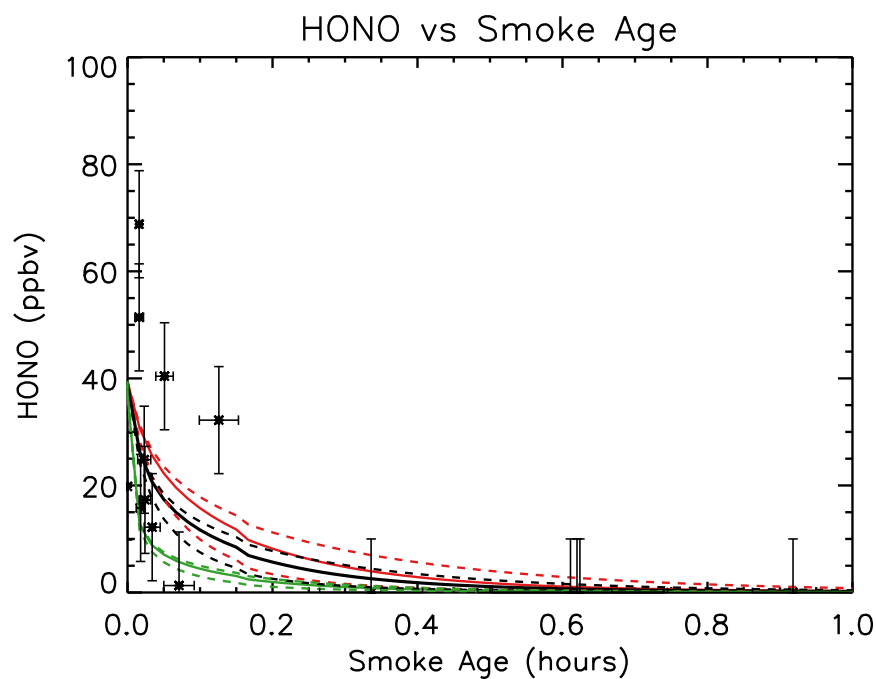
2

3 Figure 5. Enhancement ratios (mol/mol) of (a)  $O_3$  to  $CO$  and (b)  $PAN$  to  $CO_2$  versus estimated  
 4 smoke age when the chemistry of the unidentified SVOCs is not included in the model.  
 5 Asterisks are the measured mixing ratios, with the horizontal error bars showing the  
 6 uncertainty in the estimated age and the vertical error bars showing the uncertainty in the  
 7 measurement. Red, black, and green are ASP results for the slow, best-fit (medium), and fast  
 8 plume dilution rates. Dashed lines are for above-plume photolysis rates, while solid lines are  
 9 for the middle of the plume, and dotted lines are for the bottom of the plume (see the legend  
 10 in Figure 4).





1  
 2  
 3 Figure 6. (a)  $\text{NO}_x$  enhancement ratio (EnR, mol/mol) to  $\text{CO}_2$  versus estimated smoke age  
 4 when the chemistry of the unidentified SVOCs is not included in the model. (b) EnR of  $\text{C}_2\text{H}_4$   
 5 to  $\text{CO}$  versus estimated smoke age. Asterisks are the measured mixing ratios, with the  
 6 horizontal error bars showing the uncertainty in the estimated age and the vertical error bars  
 7 showing the uncertainty in the measurement. Red, black, and green are ASP results for the  
 8 slow, best-fit (medium), and fast plume dilution rates. Dashed lines are for above-plume  
 9 photolysis rates, while solid lines are for the middle of the plume, and dotted lines are for the  
 10 bottom of the plume (see the legend in Figure 4).

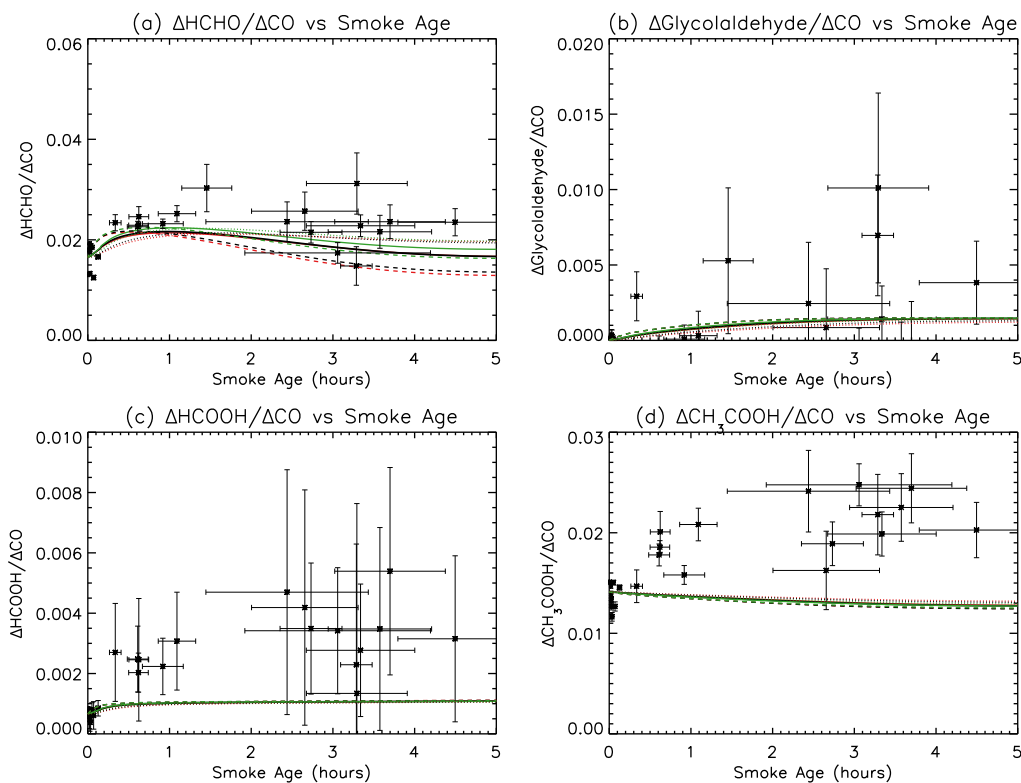


1

2

3 Figure 7. HONO mixing ratio (ppbv) versus estimated smoke age for the first hour after  
 4 emission (note difference in x-axis scale from Figures 4-6) when the chemistry of the  
 5 unidentified SVOCs and a downwind HONO source is not included in the model. Asterisks  
 6 are the measured mixing ratios, with the horizontal error bars showing the uncertainty in the  
 7 estimated age and the vertical error bars showing the uncertainty in the measurement. Red,  
 8 black, and green are ASP results for the slow, best-fit (medium), and fast plume dilution rates.  
 9 Dashed lines are for above-plume photolysis rates, while solid lines are for the middle of the  
 10 plume, and dotted lines are for the bottom of the plume (see the legend in Figure 4).

11



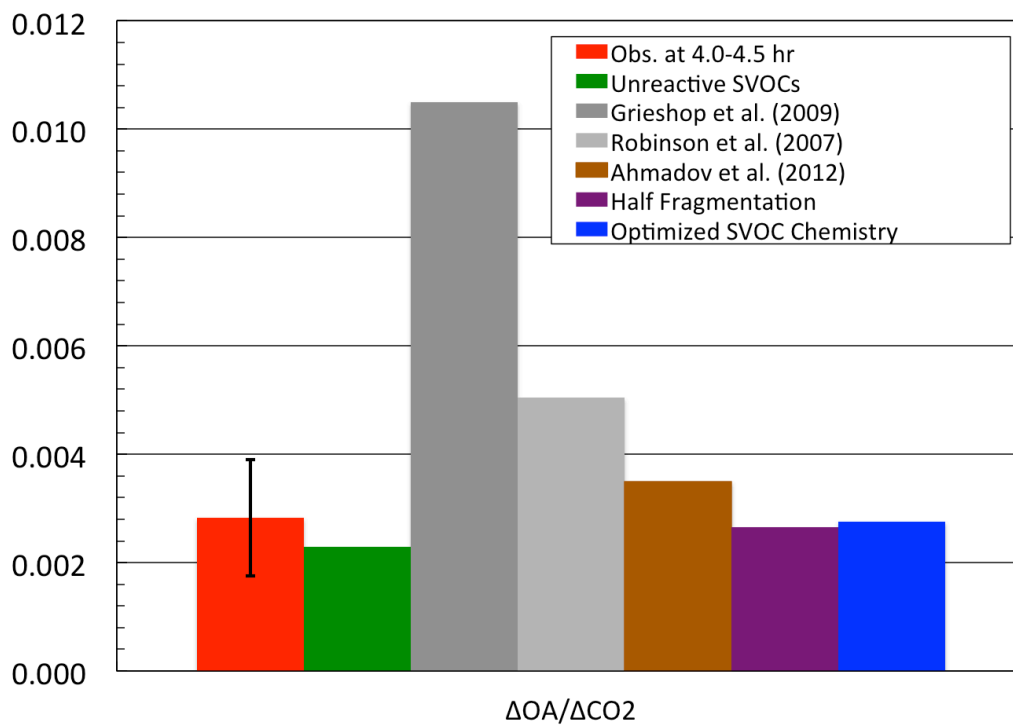
1

2

3 Figure 8. Enhancement ratio (EnR, mol/mol) of (a) HCHO, (b) glycolaldehyde (HCOCH<sub>2</sub>OH),  
 4 (c) formic acid (HCOOH), and (d) acetic acid (CH<sub>3</sub>COOH) to CO versus estimated smoke age  
 5 when the chemistry of the unidentified SVOCs is not included in the model. Asterisks are the  
 6 measured mixing ratios, with the horizontal error bars showing the uncertainty in the  
 7 estimated age and the vertical error bars showing the uncertainty in the measurement. Red,  
 8 black, and green are ASP results for the slow, best-fit (medium), and fast plume dilution rates.  
 9 Dashed lines are for above-plume photolysis rates, while solid lines are for the in-plume rates,  
 10 as described in the text.

11

12

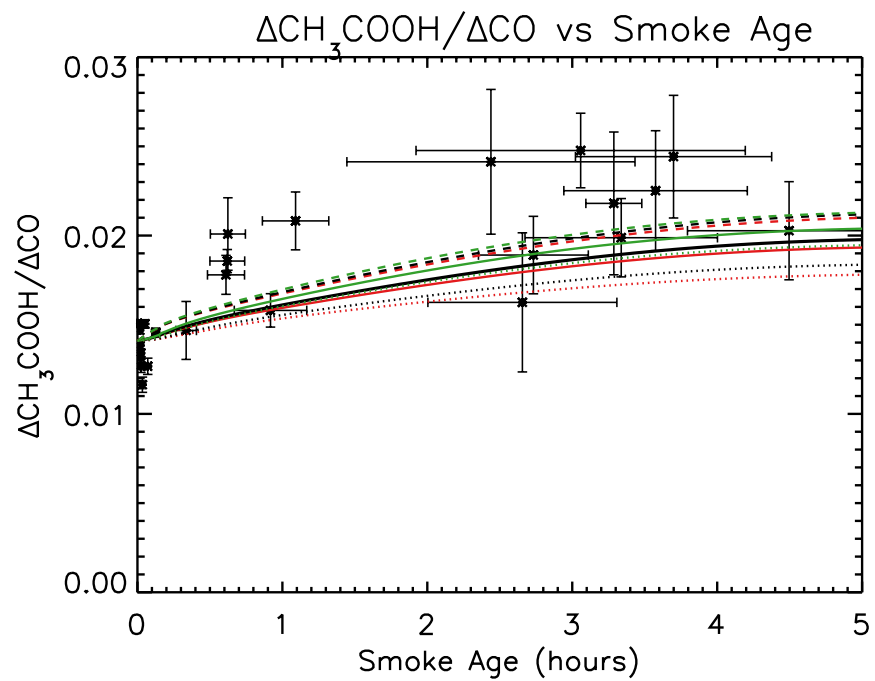


1

2

3 Figure 9. Enhancement ratio (EnR, g/g) of organic aerosol (OA) to CO<sub>2</sub> after 4 to 4.5 hr of  
 4 smoke aging. The error bars on the observed values are based on the 36% uncertainty in the  
 5 AMS observations of OA. All model results assume the best-estimate dilution rate and the  
 6 photolysis rates corresponding to the middle of the plume (solid black line in Figure 4).

7

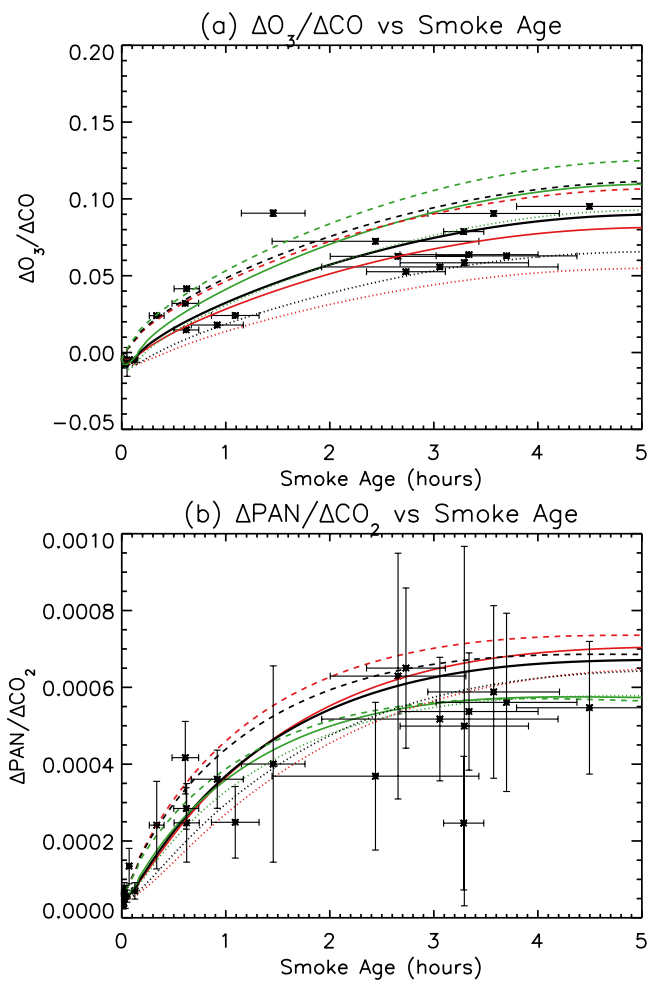


1

2

3 Figure 10. As in Figure 8d, but for the “Half Fragmentation” SVOC mechanism (see Table 1)  
 4 where the VOC fragment produced by fragmentation of the parent SVOC is assumed to  
 5 become acetic acid.

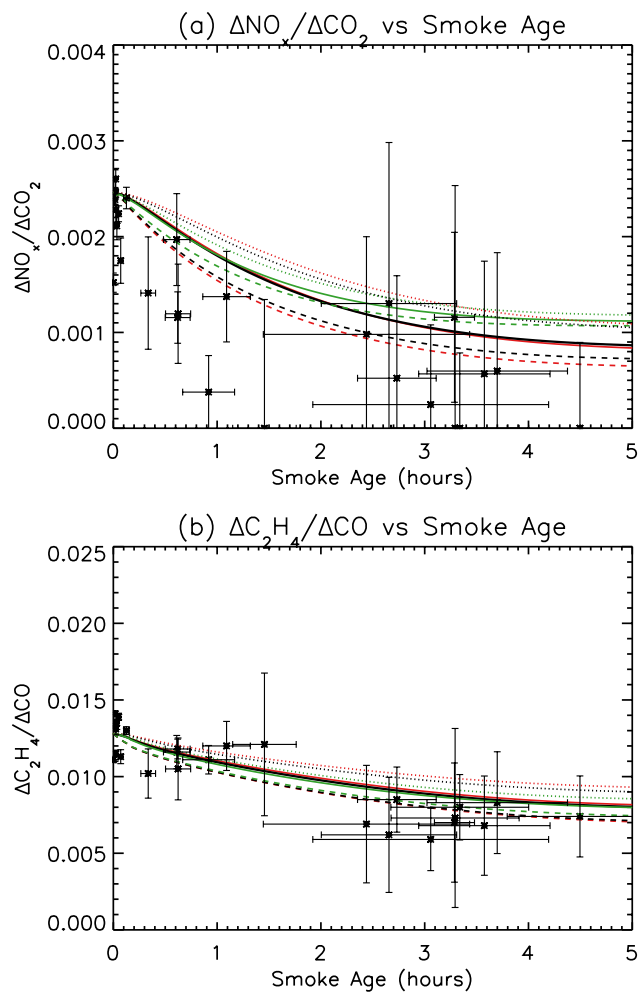
6



1

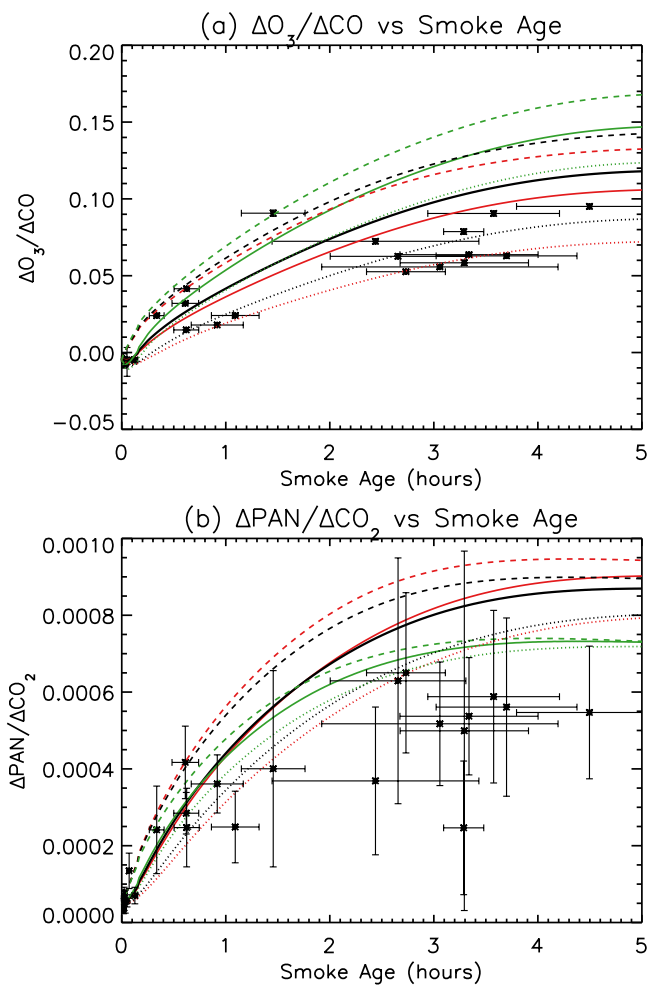
2

3 Figure 11. As in Figure 5, but for the “Half Fragmentation” SVOC mechanism rather than no  
 4 fragmentation (see Table 2).



1  
2  
3  
4  
5

Figure 12. As in Figure 6, but for the “Half Fragmentation” SVOC mechanism (see Table 2).



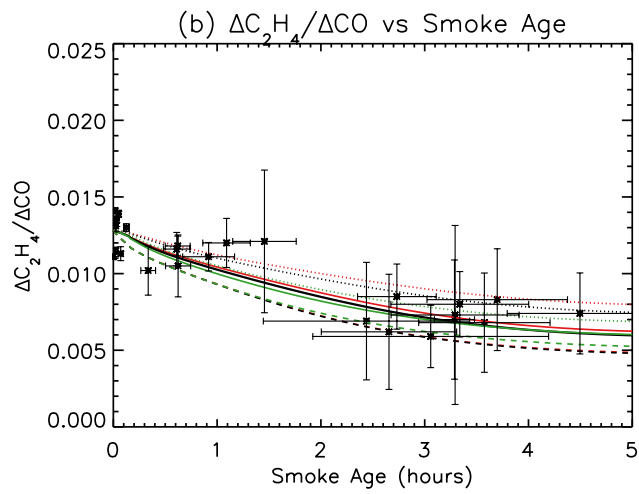
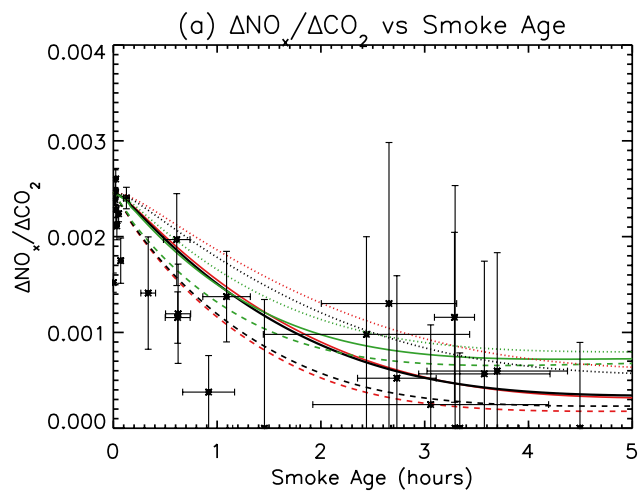
1

2

3 Figure 13. As in Figure 5, but for the optimized SVOC chemistry (see Table 2).

4





1

2

3 Figure 14. As in Figure 6, but for the optimized SVOC Chemistry (see Table 2).

4